CAPTURING PEDESTRIAN-VEHICLE CONFLICTS USING COMPUTER VISION: PREDICTING THE SEVERITY OF CONFLICTS AND EXAMINING THE EFFECTS OF PEDESTRIAN, VEHICLE AND SIGNAL TIMING-RELATED FACTORS

by

Panick Kalambay Ilunga

A dissertation submitted to the faculty of
The University of North Carolina at Charlotte
in partial fulfillment of the requirements
for the degree of Doctor of Philosophy in
Civil Engineering

Charlotte

2023

Approved by:

_____
Dr. Srinivas S. Pulugurtha

_____
Dr. Martin R. Kane

_____
Dr. Rajaram Janardhanam

_____
Dr. Monica S. Johar

ABSTRACT

PANICK KALAMBAY ILUNGA. Capturing Pedestrian-Vehicle Conflicts Using Computer Vision: Predicting the Severity of Conflicts and Examining the Effects of Pedestrian, Vehicle, and Signal Timing-related factors. (Under the guidance of DR. SRINIVAS S. PULUGURTHA)

Human driver errors are responsible for most crashes resulting from conflicts with vehicles. In the United States, 94% of crashes are attributed to human errors when driving a vehicle. According to crash statistics, the United States witnessed 6,205 pedestrian fatalities and 76,000 injuries on its roads. These numbers are still unacceptably high and urge the need for proactive measures to mitigate pedestrian-vehicle conflicts and strive toward achieving a crash-free society.

This research focuses on object detection and tracking algorithms, specifically YOLOv4 and DeepSORT, to examine pedestrian safety at a signalized intersection with a fixed cycle time and an intersection controlled by rectangular rapid flashing beacons (RRFBs). The primary objectives are threefold: first, to assess pedestrian safety; second, to predict the severity of conflicts that may arise between pedestrians and vehicles; and third, to examine the effects of various factors pertaining to pedestrians, vehicles, and signal timing on the severity of pedestrian-vehicle conflicts.

Three levels of severity of pedestrian-vehicle conflicts were defined in accordance with the established literature. The first level of severity, referred to as no conflict, is when the post-encroachment time (PET) between a pedestrian and vehicle exceeds 6s. The second level of severity, labeled as slight conflict, encompassed pedestrian-vehicle conflicts with a PET greater than 3s but not exceeding 6s. The third and most severe level of severity involved pedestrian-vehicle conflicts with a PET of 3s or less. They were detected using YOLOv4 and DeepSORT.

Two long short-term memory (LSTM) neural network models were developed for both intersections to predict the severity of pedestrian-vehicle conflicts. The LSTM neural network

models demonstrated good performance and achieved minimum recall values of 74% and 66% for slight and severe conflicts. These models can be implemented for real-time prediction of pedestrian-vehicle conflict severity. The system can warn drivers 2s ahead about a potential conflict with a pedestrian, thus fostering a proactive approach to mitigating conflicts and enhancing overall road safety.

The results also revealed that driving at a speed greater than the speed limit at the fixed-cycle intersection and the RRFB-controlled intersection increases the likelihood of a slight conflict by about 24.7% and 27.0%, respectively, compared with the non-conflict situation. Similarly, the likelihood of a severe conflict increases by 13.1% and 18.9% at the fixed-cycle intersection and the RRFB-controlled intersection, respectively, compared to the slight conflict situation. Compliance with the speed limit will lower the severity of pedestrian-vehicle conflicts at both intersections.

The findings provided insightful evidence that increasing the yellow time and the RRBF flashing time significantly lowered the severity of pedestrian-vehicle conflicts at both intersections. Compared with the non-conflict situation, a one-second extension of the yellow time and the flashing time can decrease the likelihood of a slight conflict situation by 17.2% and 21.3%, respectively. On the other hand, a one-second extension of the yellow time and the flashing time can decrease the likelihood of a severe conflict situation by about 20.9% and 19.3%, respectively in comparison to a slight conflict situation. The findings emphasize the importance of paying close attention to signal timing (especially the yellow time and the RRBF flashing time) at both fixed-cycle and RRFB-controlled intersections. These two signal timing factors should be considered as integral measures for enhancing pedestrian safety and minimizing potential conflicts with vehicles.

DEDICATION

To My Family

AKNOWLEDGMENTS

I would like to convey my deepest gratitude to my advisor, Dr. Srinivas S. Pulugurtha, for his unwavering support and invaluable guidance throughout my Ph.D. program. I am forever indebted to him for instilling in me the profound significance of commitment in my academic pursuits. His continual encouragement and personalized mentorship have provided me with an unparalleled learning experience, exceeding all my expectations as an individual. Dr. Srinivas, I extend my heartfelt appreciation to you for bestowing upon me the invaluable opportunity to pursue a Ph.D. under your exceptional guidance.

A special word of thanks to the esteemed members of my committee: Dr. Martin R. Kane, Dr. Rajaram Janardhanam, and Dr. Monica S. Johar. Their suggestions have played an instrumental role in enhancing the quality and depth of my dissertation. I am grateful for their invaluable contributions, which have undoubtedly enriched my research journey.

I would also like to thank the North Carolina Department of Transportation (NCDOT) for the financial support of my dissertation through the NC Transportation Center of Excellence in Advanced Technology Safety and Policy. Additionally, I extend my thanks to Mr. Andrei Dumitru of the city of Concord, North Carolina, for his assistance and support with the data collection.

I would also like to thank my fellow student researchers. Working alongside them has been a pleasure, as we shared a passion for transportation engineering. I am thankful for the experiences forged working together in the Infrastructure, Design, Environment, and Sustainability (IDEAS) Center.

Lastly, my grateful appreciation to my family for their support and unconditional love. Their constant encouragement, understanding, and sacrifices have been the pillars that have

supported me throughout my journey. I am deeply grateful for always being my rock and providing the strength and encouragement that have allowed me to pursue my dreams. Thank you, from the bottom of my heart to my incredible family for being my foundation and guiding light.

TABLE OF CONTENTS

LIST OF TABLES

LIST OF FIGURES

LIST OF ABBREVIATIONS

AC	Adjacent Category
ACPPC	Adjacent Category with Partial Proportional Constraints
ARIMA	Autoregressive Integrated Moving Average
AUC	Area Under Curve
CAV	Connected and Automated Vehicle
CNN	Convolutional Neural Network
COCO	Common Object in Context
F-RCNN	Faster Region-based Convolutional Neural Network
FN	False Negative
FP	False Positive
GRU	Gated Recurrent Unit
IoU	Intersection over Union
LSTM	Long Short-Term Memory Network
MOT	Multiple Object Tracking
MRE	Mean Relative Error
NC	North Carolina
NCSA	National Center for Statistics and Analysis
PET	Post-Encroachment Time
PPO	Partial Proportional Odds
PO	Proportional Odds
R-CNN	Region-based Convolutional Neural Network

RAE	Relative Accuracy Error
RNN	Recurrent Neural Network
ROI	Region of Interest
ROW	Right-of-Way
RPE	Relative Precision Error
RRFB	Rectangular Rapid-Flashing Beacon
SMOTE	Synthetic Minority Over-Sampling Technique
SORT	Simple Online and Real-Time Tracking
SOT	Single Object Tracking
SSM	Surrogate Safety Measure
TN	True Negative
TP	True Positive
TTC	Time-to-Collision
YOLO	You Only Look Once

CHAPTER 1: INTRODUCTION

1.1. Motivation and Background

Previous research extensively assessed pedestrian-vehicle interactions and revealed their vital role in smooth and efficient traffic flow, as well as improving safety (Rasouli and Tsotsos, 2018; Fuest et al., 2017; Zhang et al., 2017; Lehsing et al., 2016; Haddington and Rauniomaa, 2014; Jensen, 2010). However, the number of traffic crashes in the U.S., and elsewhere in the world remains unacceptably high. On average, 2,046,000 traffic crashes are reported annually. About 94% of the total number of traffic crashes at the national level are due to human driver errors (Singh, 2018). In 2019, 6,205 pedestrians were killed, and 76,000 were injured in traffic crashes (NCSA, 2020).

Pedestrian crashes are most frequent in urban areas, with intersections being particularly prone to pedestrian-vehicle conflicts compared to other road facilities, as reported by Zhang and Abdel-Aty (2022). Over the years, in-depth assessments have been conducted at intersections to comprehensively assess the effectiveness of diverse safety countermeasures in improving pedestrian safety. These countermeasures include pedestrian countdown signals, pedestrian refuge islands, leading pedestrian intervals, and a range of conventional strategies (Pulugurtha and Self, 2015; Pulugurtha et al., 2011; Vasudevan et al., 2011; Dangeti et al., 2010; Pulugurtha et al., 2010a; Pulugurtha et al., 2010b; Nambisan et al., 2009; Karkee et al., 2006).

The conventional approach to road safety analysis is predominantly reactive in nature, relying heavily on crash data or vehicular crash reconstruction, as noted by Tarko (2018). This reactive approach poses inherent limitations, as researchers must wait for crashes to occur before taking preventive measures. Furthermore, relying solely on crash data may not provide a

comprehensive or accurate understanding of the underlying factors contributing to these crashes, thus hindering the development of effective safety strategies. In contrast, the proactive nature of traffic conflict theory offers a promising alternative. By utilizing surrogate safety measures (SSMs) such as post-encroachment time (PET), potential hazards can be identified proactively before actual crashes transpire (Tarko, 2018). Islam et al. (2014) found that minor and serious conflicts are marginally significant in predicting total pedestrian crashes and are good surrogate safety for crashes.

With the continuous advancement of computer vision technologies, the field of traffic safety analysis, especially pedestrian-vehicle interactions, is undergoing a significant transformation toward automated methods for pedestrian and vehicle detection and tracking. These innovative technologies are paving the way for the future of connected and automated vehicles (CAVs), wherein vehicles equipped with advanced features can detect and track pedestrians and other vehicles. The introduction of such technologies holds the potential to mitigate human errors that contribute to crashes, including instances of drunk driving, distracted driving, aggressive driving, and failures to perceive pedestrians, even those who jaywalk. As a result, implementing these technologies has the potential to significantly enhance road safety, leading to a future where roads are considerably safer than they are at present.

As we transition toward a CAV environment, it is crucial to acknowledge that further research and development are essential to guarantee the reliability and effectiveness of these technologies in preventing pedestrian crashes. Therefore, ongoing research in this domain is of utmost importance to fully harness the potential benefits of these innovative technologies and ensure enhanced safety on our roads for all users.

1.2. Problem Statement

To better handle the issues mentioned in Section 1.1, i.e., to overcome the reactive nature of crash data, video data needs to be explored as it emerges as the most effective source for assessing pedestrian-vehicle conflicts, offering a microscopic view of real-world traffic scenes. This sets it apart from other data sources like radio detection and ranging, loop detectors, and Bluetooth sensors (Zhang et al., 2020a; Ka et al., 2019; Wu et al., 2019; Wang et al., 2012). Moreover, the fact that pedestrians and drivers are often unaware of being recorded allows for more naturalistic observations of the communication dynamics between pedestrians and vehicles, facilitating an ex-ante assessment of the risks posed by evasive actions from both the parties.

Despite the implementation of signalized intersections, which provide a relatively favorable crossing environment by allowing pedestrians to cross during allocated green time, urban areas continue to face persistent challenges related to pedestrian safety. Pedestrian-vehicle conflicts represent a significant safety concern, particularly at signalized intersections, which are critical areas within urban environments (Alhajyaseen and Iryo-Asan, 2017; Iryo-Asano et al., 2014; Bradbury et al., 2012). These intersections serve as hotspots where the movements of pedestrians and vehicles intersect, leading to a higher likelihood of conflicts. According to Ewing and Dumbaugh (2009), conflicts are one of the three primary factors contributing to traffic crashes. It is important to note that conflicts can still arise at intersections even with the presence of traffic signals. These conflicts manifest in various ways, such as conflicts between pedestrians and left or right-turning vehicles within a single phase, where their movements may intersect. Additionally, conflicts can occur between different phases of the signal cycle when pedestrians may not have sufficient time to complete their crossing of the intersection (Chen et al., 2014).

One prominent issue is the prevalence of jaywalking, where pedestrians choose to cross streets outside designated crosswalks or against traffic signals. These challenges not only compromise the safety of pedestrians but also contribute to the complexity of urban traffic management. Jaywalking and non-compliance with traffic signals create conflicts with vehicular traffic, leading to increased risks of crashes and disruptions to the overall traffic flow. In addition, the issue related to pedestrian-vehicle conflicts at fixed-cycle intersections or rectangular rapid flashing beacons (RRFBs)-controlled intersections in urban areas is not solely influenced by pedestrian behavior but also by other factors, such as vehicle speeds, signal timing-related factors, and traffic flow patterns, that may play a significant role in shaping the incidence of conflicts between pedestrians and vehicles.

The research discussed here serves as a step forward, using advanced automated detection and tracking techniques to analyze video data and assess pedestrian-vehicle conflicts, specifically at fixed-cycle intersections and RRFB-controlled intersections. It addresses the pressing need for improved safety measures in urban areas, contributing to the broader goal of creating safer and more secure road environments.

1.3. Research Objectives

The objectives of this research, therefore, are:

1. to extract pedestrian and vehicle data by employing advanced detection and tracking algorithms on video recordings captured at a fixed-cycle intersection and a RRFB-controlled intersection,
2. to assess the temporal relationship between pedestrians and vehicles, i.e., pedestrian-vehicle conflicts using SSMs such as PET,

3. to predict conflict severity between pedestrians and vehicles by considering various factors such as pedestrian behavior, vehicle characteristics, and signal timing phases, and
4. to examine the effects of the pedestrian, vehicle, and signal timing factors on the severity levels of pedestrian-vehicle conflicts. Specifically, the focus will be on understanding how these factors contribute to adjacent levels of conflict severity.

1.4. Dissertation Structure

The rest of the dissertation is structured as follows. Chapter 2 presents a literature review on pedestrian-vehicle communication, pedestrian-vehicle conflicts, the potential application of detection and tracking algorithms for traffic safety purposes, and the effects of pedestrian, vehicle, and signal timing factors on pedestrian-vehicle conflicts. Identified research gaps are then discussed and drive the following chapters. Chapter 3 outlines the methodological approach used in this research. Chapter 4 details the data collection and processing undertaken in this research. Chapter 5 and Chapter 6 focus on assessing pedestrian safety at a fixed-cycle intersection and an RRFB-controlled intersection, respectively. Chapter 7 and Chapter 8 discuss the effects of pedestrian, vehicle, and signal timing factors on the severity levels of pedestrian-vehicle conflicts occurring at the fixed-cycle intersection and the RRFB-controlled intersection, respectively. Chapter 9 presents the conclusions from this research and the scope for future research.

CHAPTER 2: LITERATURE REVIEW

A comprehensive review of existing literature is presented in this chapter. The review covers topics such as pedestrian-vehicle communication, pedestrian-vehicle conflicts, and the potential application of detection and tracking algorithms for traffic safety. It also examines the influence of pedestrian, vehicle, and signal timing factors on the occurrence and severity of pedestrian-vehicle conflicts. By identifying and assessing these factors, the literature review establishes a solid foundation for the subsequent chapters, providing valuable insights and illuminating key research gaps that need to be addressed.

2.1. Communication between Pedestrians and Vehicles

Clear and effective communication is crucial between pedestrians and vehicles, particularly at intersections where conflicts between pedestrian and vehicle movements are prone to occur. This communication occurs through both pedestrian-to-vehicle and vehicle-to-pedestrian communication, ensuring mutual awareness and facilitating safe interactions in the road space.

2.1.1. Pedestrian-to-Vehicle Communication

During the negotiation of the right-of-way (ROW), human drivers rely on interpreting non-verbal cues from pedestrians to facilitate communication. Pedestrians often convey their intentions through various non-verbal cues, including glance or gaze in the direction of the vehicle and hand gesturing to signal their intentions. Additionally, the body pose of a pedestrian standing at the curb can also indicate their intention to cross the road.

Establishing eye contact is a common practice among pedestrians before crossing a road. It is generally presumed that pedestrians feel acknowledged and safe when drivers reciprocate this eye contact (Schmidt and Färber, 2009). However, when traffic signals or stop signs are present, pedestrians may be less inclined to establish eye contact with oncoming traffic, as they rely on the expectation that drivers will adhere to traffic rules (Rasouli and Tsotsos, 2018).

In addition to being efficient, hand gesturing is the most easily interpretable and explicit non-verbal cue used among road users (Färber, 2016; Zhuang and Wu, 2014). Pedestrians can use hand gestures to convey gratitude or request the ROW depending on the situation.

2.1.2. Vehicle-to-Pedestrian Communication

Drivers have the option to either come to a complete stop to yield the ROW to pedestrians or indicate explicitly, through cues such as hand gestures or other visual signals, that they have detected pedestrians and it is safe for them to proceed (Song et al., 2018; Färber, 2016; Gough, 2016). A good understanding of these cues guarantees safe interactions between pedestrians and vehicles and could serve as a basis for developing collision avoidance concepts in a CAV environment.

Such explicit communication includes the use of auditory signals such as horns, visual signals through indicators, emergency lights, warning lights, and brake lights, as well as designations such as ambulance or police (Fuest et al., 2017; Sucha et al., 2017; Färber, 2016). Additionally, labeling a vehicle as a CAV can also serve as a form of explicit communication (Fuest et al., 2017). However, the relevance of this form of communication diminishes as vehicle speed increases, leading to a reduced impact on overall road safety for several reasons (Färber, 2016). Firstly, drivers may not be able to perceive or respond to pedestrian reactions at higher

speeds due to the limited time available for observation and reaction. Additionally, the time required for pedestrians to react and respond becomes significantly longer, making it challenging to synchronize their actions with vehicles traveling at high speeds.

In summary, pedestrian-to-vehicle communication and vehicle-to-pedestrian communication are critical to ensuring safety and efficiency in urban environments. Effective communication between pedestrians and vehicles can substantially reduce the risk of conflicts and their severity and enhance overall traffic flow. Detection and tracking algorithms provide a foundation for developing advanced systems that facilitate real-time communication between pedestrians and vehicles, allowing for proactively avoiding potential conflicts.

2.2. Object Detection and Tracking for Pedestrian-Vehicle Conflicts

Computer vision techniques have revolutionized the ability to detect, count, and track pedestrians and vehicles in the road environment, predominantly leveraging deep learning-based methods. The detection process involves classifying, localizing, and visualizing pedestrians and vehicles using bounding boxes. Concurrently, tracking entails assigning unique and consistent identities to individuals over time, enabling continuous monitoring.

In this research, the combined approach, known as tracking-by-detection, is used. It combines both techniques to detect pedestrians and vehicles in each frame of a video sequence and link the detections across frames to accurately track their movements.

2.2.1. Object Detection and Tracking Algorithms

Object detection algorithms can be classified into two categories based on their approach. Two-stage algorithms, such as region-based convolutional neural networks (R-CNN) (Girshick et

al., 2014) and faster R-CNN (F-RCNN) (Ren et al., 2015), involve selecting regions of interest (ROI) and applying a CNN for object detection. On the other hand, one-stage algorithms like You Only Look Once (YOLO) (Redmon et al., 2016) predict object classes and bounding boxes for the entire image without the need for ROI selection. While two-stage algorithms generally offer higher detection accuracy (Krishna et al., 2021), one-stage algorithms like YOLO (Chahal and Dey, 2018) are faster and more efficient, making them well-suited for real-time applications.

Object tracking can be divided into two categories: single-object tracking (SOT) and multiple-object tracking (MOT) (Koller-Meier, 2001). SOT focuses on estimating the trajectory of a single object over time, while MOT involves tracking multiple objects simultaneously. Both SOT and MOT present their own unique challenges. However, specific algorithms have been developed to address these challenges. For instance, Simple Online and Realtime Tracking (SORT) (Bewley et al., 2016) utilizes CNN-based object detectors to achieve real-time processing, while DeepSORT (Wojke et al., 2017) enhances tracking performance by preventing the assignment of a new detection identity to an already tracked object. DeepSORT has demonstrated exceptional results on various benchmarks, showcasing its effectiveness in MOT scenarios.

2.2.2. Predicting the Severity of Pedestrian-Vehicle Conflicts using Object Detection and Tracking

There is more and more research that employs object detection and tracking techniques to facilitate automated pedestrian safety assessments, utilizing a range of SSMs (Ali et al., 2023; Zhang et al., 2020a; Zhang et al., 2020b; Zangenehpour et al., 2015; Hussein et al., 2015). These measures act as valuable proxies for safety, enabling the assessment and quantification of potential risks and hazards encountered by pedestrians in diverse road environments.

In their work, Zangenehpour et al. (2015) proposed a methodology that significantly enhanced the detection, classification, and tracking of moving objects in complex traffic scenes, encompassing pedestrians and vehicles. This approach achieved an impressive overall classification accuracy of 88%.

Similarly, Hussein et al. (2015) conducted a study on diagnosing pedestrian safety issues by identifying contributing factors. They successfully demonstrated the feasibility of automatically extracting pedestrian data for behavior analysis, including speed and gait parameters. Their findings indicated that pedestrian violations, especially temporal violations such as crossing during the Don't Walk or flashing Don't Walk phase, were the primary factor contributing to the high number of conflicts between pedestrians and vehicles.

Zhang et al. (2020a) proposed a methodology to predict pedestrian-vehicle conflicts and classify unsafe situations at a signalized intersection. The approach used PETs and employed a long short-term memory (LSTM) neural network (Hochreiter and Schmidhuber, 1997). By analyzing the PET values, the model classified severe conflicts (PET $\leq$ 3s), slight conflicts (3s < PET $\leq$ 6s), and no conflicts. The research achieved an impressive overall accuracy of 88.5% in distinguishing between these conflict categories. Additionally, Zhang et al. (2020b) used the minimum time-to-collision (TTC) to predict near-crash events between pedestrians and vehicles at signalized intersections. This was accomplished by employing gated recurrent unit (GRU) neural networks. The model successfully identified potential near-crash events by analyzing the minimum TTC values. They achieved an overall accuracy of 87.8% in distinguishing severe conflicts (minimum TTC $\leq$ 3s), slight conflicts (3s < minimum TTC $\leq$ 6s), and no conflicts.

In a more recent research, Ali et al. (2023) presented a real-time framework to estimate crash risk at the signal cycle level. Their innovative approach involved the use of an automated

extraction algorithm that combined data from the trajectory, traffic conflict, and signal timing databases. By integrating these datasets, the framework obtained signal cycle-level covariates, enabling a comprehensive understanding of the time-varying risk associated with severe pedestrian-vehicle conflicts across different signal cycles.

2.3. Effects of Pedestrian, Vehicle, and Signal Timing-related Factors on Pedestrian-Vehicle Conflicts

This section of the literature review summarizes the effects of pedestrian, vehicle, and signal timing-related factors on the occurrence and severity of pedestrian-vehicle conflicts. It explores the relationships between these factors and their influence on pedestrian-vehicle conflicts. Additionally, it discusses various models developed to measure these effects, enabling researchers and policymakers to better understand the dynamics of pedestrian-vehicle conflicts and implement effective measures to mitigate them.

2.3.1. Effects of Pedestrian-Related on Pedestrian-Vehicle Conflicts

The likelihood of pedestrian-vehicle conflicts at intersections can be influenced by several factors, including the direction of pedestrian travel (Hubbard et al., 2009), pedestrian age (Hu et al., 2020a), gender (Hu et al., 2020b), pedestrian volume and time of the day (Pulugurtha et al., 2006). Pulugurtha and Repaka (2008) developed models to measure pedestrian activities in urban areas by the time of the day.

Conflicts are more likely to occur when pedestrians arrive or start crossing late, such as towards the end of the designated walk interval, particularly during the green time for right-turning vehicles (Hubbard et al., 2009). Furthermore, conflicts can arise between different phases of the

signal cycle when pedestrians are given insufficient time to complete their crossing of the intersection (Chen et al., 2014). Crashes involving pedestrians at intersections, especially those controlled by traffic signals, often involve a vehicle attempting to clear the intersection and inadvertently colliding with a pedestrian crossing the road (Chen et al., 2014).

Green et al. (2023) conducted a study to examine the impact of exclusive phase signals on the occurrence of conflicts. Their findings revealed that implementing exclusive phase signals resulted in an 85% reduction in the odds of conflicts. The research analyzed two significant variables: the time required for pedestrians to cross the road and the waiting time before crossing. These variables were identified as crucial factors affecting the likelihood of conflicts between pedestrians and vehicles.

Zhang et al. (2015) conducted a study that revealed exclusive pedestrian phasing is only safer for pedestrians when they choose to wait for the designated "Walk" signal. Bradbury et al. (2012) demonstrated that pedestrians were more likely to wait for the signal to indicate "Walk" if they used a pedestrian call button. However, even in areas equipped with RRFBs, jaywalking may still occur, particularly when crosswalk locations are inconvenient for pedestrians. Therefore, strategies such as pedestrian call buttons or RRFBs should be tailored to the location to increase the likelihood of pedestrians utilizing them effectively and adhering to designated crossing procedures.

Nevertheless, RRPB systems offer advantages compared to traditional pedestrian call buttons. Bradbury et al. (2012) found that pedestrians have greater trust in the RRFB system, as they perceive that activating the device will reliably result in a flashing yellow signal. This enhanced trust in the RRFB can positively influence pedestrian behavior and adherence to signal indications. In fact, pedestrians prioritize low wait times and efficient crossing durations when

utilizing pedestrian facilities. These factors are highly valued by pedestrians and are associated with a decrease in the likelihood of conflicts, as supported by the findings of Green et al. (2023).

2.3.2. Effects of Vehicle-Related Factors on Pedestrian-Vehicle Conflicts

Vehicles are bound to operate within designated lanes than pedestrians, making their movements more predictable. As a result, drivers tend to exhibit relatively fewer evasive actions than pedestrians. Therefore, the most significant factors affecting pedestrian safety revolve around vehicle speeds.

Zhang et al. (2015) conducted a study in which they modeled pedestrian-vehicle conflicts and observed that the number of potential conflicts decreased at lower speeds (25 mph) compared to higher speeds (35 mph). This finding highlights the influence of vehicle speeds on the occurrence of conflicts. They suggest that reducing vehicle speeds can play a crucial role in enhancing pedestrian safety. By enforcing lower speed limits in areas with high pedestrian activity, the potential for conflicts can be mitigated, providing pedestrians with a safer environment to cross roads.

Previous research showed that increased traffic flow and the number of approach lanes at intersections are associated with a higher likelihood of observing red-light violations. Red-light running is also common practice, especially in cities with wider intersections and higher traffic volumes (Pulugurtha and Otturu, 2014; Porter and England, 2000). Karinpour et al. (2023) conducted research in this area and found a positive correlation between these factors. As traffic volume intensifies and the number of lanes at an intersection increases, drivers are at an elevated risk of disregarding red signals, leading to increased likelihood for conflicts with pedestrians or other vehicles.

2.3.3. Effects of Signal Timing-Related Factors on Pedestrian-Vehicle Conflicts

As mentioned previously, signal timing-related factors can affect pedestrian-vehicle interactions at signalized intersections. The timing parameters of signal phases, such as green time, yellow time, and red time intervals, can significantly impact the safety and efficiency of pedestrian movements.

Zhang et al. (2015) recommended that exclusive pedestrian phasing be installed at locations where pedestrians are more likely to comply. They examined a sample of signalized intersections in Connecticut, considering the presence of concurrent or exclusive pedestrian phasing. They found that pedestrians crossing on the walk signal at an exclusive signal encountered lower interaction severity than crossing on the green light with concurrent phasing. However, pedestrians crossing on a green light with an available exclusive phase experienced higher interaction severity. Moreover, intersections with concurrent phasing exhibit fewer total pedestrian crashes than those with exclusive phasing but more crashes at higher interaction severity.

Agbelie and Roshandeh (2014) conducted a study that revealed an interesting relationship between the number of signal phases and crash frequency at intersections. According to their findings, a unit increase in signal phases was associated with a 0.4 increase in crash frequency. This suggests that an increase in signal timing complexity, such as including additional signal phases, may contribute to a higher likelihood of crashes occurring at intersections.

Increasing the cycle length to provide pedestrians with more time to cross can be beneficial, particularly for older individuals with slower walking speeds. By extending the pedestrian crossing time, this approach caters to the needs of pedestrians, ensuring they have sufficient time to navigate the intersection safely. However, there are some drawbacks to consider. For example, increasing

the cycle length results in longer red signals for vehicles on the main street, leading to potential delays and the accumulation of longer queues during peak periods. This can impact traffic flow and overall intersection efficiency. Furthermore, the extended waiting time for pedestrians at the cross street can lead to impatience, prompting some pedestrians to cross against the signal. This behavior poses risks and can compromise pedestrian safety.

While increasing the total cycle length might be effective in promoting pedestrian safety, it was found to have an insignificant impact on motorist safety (Chen et al., 2014). Therefore, it is crucial to carefully consider the trade-offs and balance the needs of pedestrians and motorists when determining the appropriate cycle length for signalized intersections. Effective management of signal timings and pedestrian crossings can help achieve a balance that prioritizes safety for all road users while minimizing congestion and delays.

Bonneson and Zimmerman (2004) conducted research in Texas that yielded significant findings regarding the impact of yellow time on pedestrian red-light violations. According to their research, increasing the duration of the yellow light resulted in a 50% reduction in the total number of pedestrian red-light violations. This suggests that providing motorists with a longer yellow phase offers more time to respond safely and make appropriate decisions at signalized intersections.

In another research conducted in Pennsylvania, Retting et al. (2008) investigated the effects of extending the duration of the yellow light by one second at six major intersections. The results of this research demonstrated a decrease of 36% in pedestrian red-light violations. This highlights the importance of optimizing the duration of the yellow light as an effective measure to improve compliance with traffic signals and reduce risky behaviors at intersections.

2.3.4. Modeling the Effects on Pedestrian-Vehicle Conflicts

Research focusing on crash severity using crash data has been more prevalent. The literature has relatively limited research on the effects of pedestrian, vehicle, and signal timing factors on the severity of pedestrian-vehicle conflicts. Within this context, four significant research papers were identified as relevant to this research (Green et al., 2023; Hu et al., 2022; Zhang et al., 2015; Islam et al., 2014).

Green et al. (2023) employed logistic regression analysis to investigate whether there is a significant distinction in the severity of pedestrian-vehicle interactions between side street green and exclusive phase pedestrian signals. They aimed to assess the significance of waiting time and crossing time as predictors of pedestrian-vehicle conflicts. The model considered four distinct severity levels: undisturbed passage, potential conflict, minor conflict, and serious conflict. Following the interpretation of the results from six different logistic regression refinements, it was determined that waiting time, crossing time, the number of lanes, annual average daily traffic, pedestrian compliance, phasing, and the presence of crosswalks are valuable predictors in assessing pedestrian-vehicle conflicts.

Hu et al. (2022) developed an ordered probit model to examine the risk factors associated with severities of conflicts between pedestrians and vehicles. The results revealed a significant correlation between the severity level and various factors such as pedestrian behavior, vehicle characteristics, and the nature of the conflict. Additionally, they found that roadway characteristics significantly influenced the likelihood of severe pedestrian-vehicle conflicts in addition to the factors mentioned previously.

Zhang et al. (2015) fitted the generalized logit, proportional odds (PO), and partial proportional odds (PPO) models to predict the severity of pedestrian-vehicle conflicts at both

concurrent and exclusive pedestrian crossings. The conflicts were categorized into three levels based on increasing severity: undisturbed passage, potential conflict, and minor or severe conflict. The results revealed that pedestrians who crossed during the walk phase at an exclusive signal experienced lower levels of interaction severity than those crossing at a green light with concurrent phasing.

Islam et al. (2014) researched on analyzing pedestrian conflicts and crash counts to identify the exposure measures and roadway characteristics that impact pedestrian safety. To achieve this, they developed negative binomial and PO models for conflict severity and pedestrian counts. They found that minor and serious conflicts, in combination with variables such as crossing distance and building setback, are significant variables for determining the total number of pedestrian-related crashes.

2.4. Limitations of the Past Research

Past studies have emphasized the importance of leveraging innovative technologies to enhance road safety, particularly for vulnerable road users like pedestrians, whose safety remains a significant challenge. To address this need, this research employed advanced automated detection and tracking techniques to analyze video data and assess pedestrian-vehicle conflicts at a signalized intersection using SSMs, therefore addressing the need for improved safety measures in urban areas toward a CAV environment. Such a combination of automated detection with tracking of pedestrians and vehicles using SSMs has not been widely explored in previous research.

Specifically, this research aimed to assess the safety of pedestrians, including those who engaged in jaywalking at two distinct locations: a signalized intersection and an RRFB-controlled

intersection. A RRFB is a type of pedestrian-activated traffic control device that uses a pair of rapidly flashing LED lights arranged in a rectangular shape. It is typically installed at pedestrian crosswalks to enhance visibility and alert drivers to the presence of pedestrians. By examining pedestrian behavior and interactions with these two different infrastructure setups, the research aimed to gain a comprehensive understanding of safety concerns and identify potential improvements to enhance the well-being of pedestrians in both the scenarios.

Additionally, the research aimed to develop traffic conflict prediction models based on LSTM, a type of recurrent neural network. The main purpose of these models is to accurately forecast and categorize the level of conflict between pedestrians and vehicles at two specific intersections based on vehicle and pedestrian trajectories. The research seeks to enhance the accuracy of predictions and improve the categorization of conflicts for better understanding and mitigation of potential risks.

Moreover, this research aimed to address the gap in the literature that solely examined the effects of pedestrian, vehicle, and signal timing-related factors on the severity of pedestrian-vehicle conflicts based on a reference category (no pedestrian-vehicle conflict). This research proposes an adjacent-category approach that captures the relationships and differences between adjacent categories, such as the transition from no conflict to slight conflict and from slight to severe conflict. Considering these transitions in conflict severity, this research aims to provide a more comprehensive understanding and assessment of factors influencing adjacent levels of pedestrian-vehicle conflict severity.

LSTM and adjacent-category models will provide valuable insights into potential safety hazards at signalized intersections and RRFB-controlled intersections and emphasize the necessity of enhancing infrastructure safety measures and upgrading CAV technologies. By combining the

predictive capabilities of LSTM models with the comprehensive analysis provided by adjacent-category models, policymakers and stakeholders can make informed decisions to improve intersection safety and promote advancements in CAV technology.

CHAPTER 3: METHODOLOGY

The methodology used in this research encompassed three key components: (i) the extraction of video data by detecting and tracking pedestrians and vehicles, (ii) the assessment of pedestrian safety, and (iii) the prediction of pedestrian-vehicle conflicts. A visual representation of this methodology is presented in Figure 1, and the subsequent subsections provide a detailed explanation of each step.

By following this structured approach, the research aimed to gather relevant data, evaluate pedestrian safety, and forecast potential conflicts between pedestrians and vehicles based on variables pertaining to pedestrian, vehicle, and signal timing-related factors.

The video data was extracted frame by frame using advanced automated detection and tracking algorithms. This process generated pedestrian and vehicle trajectories, allowing for detailed analysis. The pedestrian safety component of the methodology concentrated on assessing conflict risks at the signalized intersection and an RRFB-controlled intersection. This assessment was based on average vehicle speeds and PET. The final step involved predicting the level of pedestrian-vehicle conflicts. In this step, PET was utilized as the dependent variable, and various variables were considered. These variables included pedestrian gender, pedestrian crossing direction, instances of jaywalking, pedestrian red-light violation, pedestrian location, vehicle location, vehicle speed, vehicle travel direction, and others. Two sets of models are developed using the R software (R Core Team, 2023). First, a trajectory-based method, LSTM neural network model, is developed to forecast pedestrian-vehicle conflicts based on the abovementioned variables. Second, the adjacent-category approach is used to determine the likelihood of the

severity of pedestrian-vehicle conflicts and capture the nuances and patterns that occur as conflicts escalate in severity.

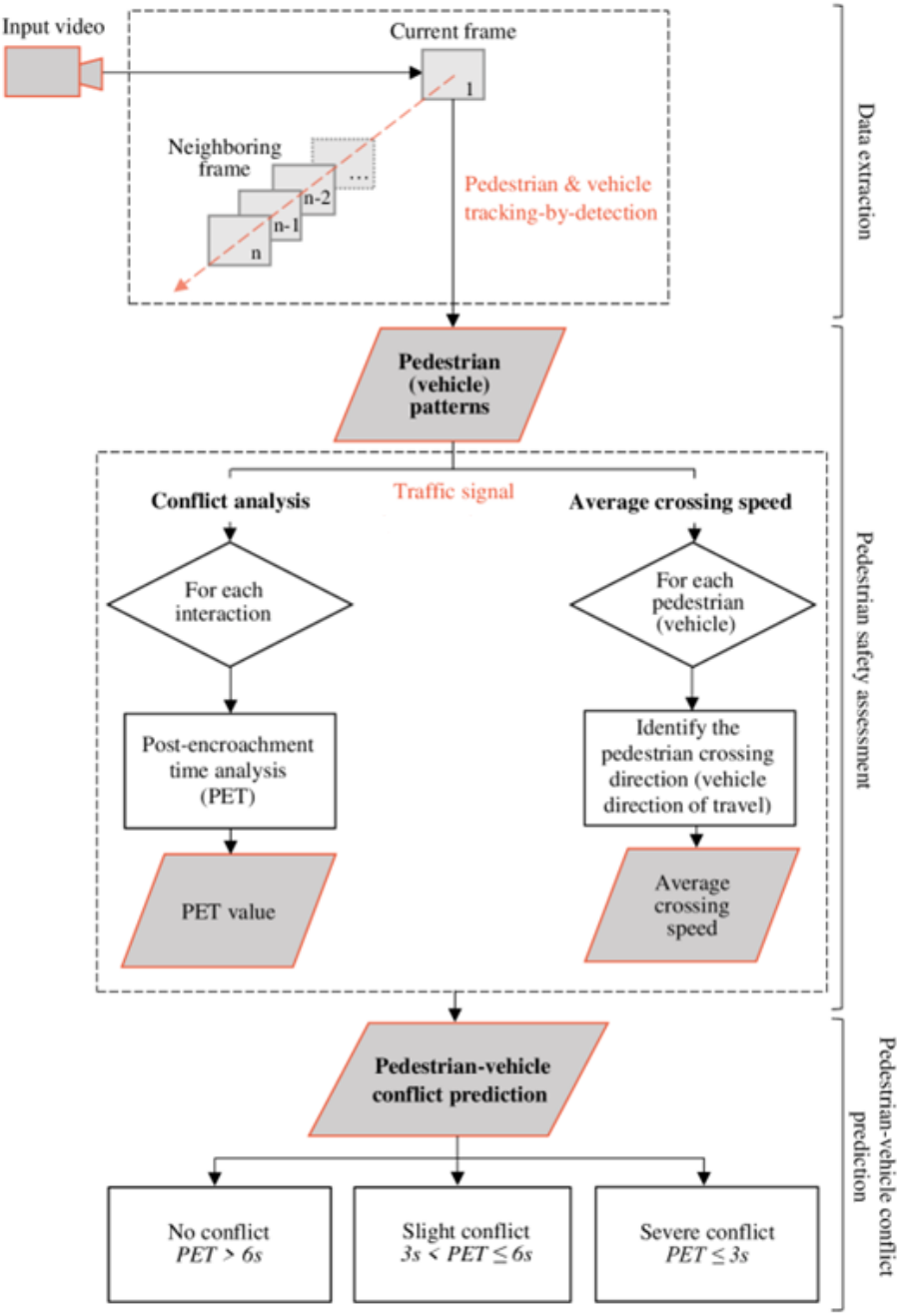

Figure 1. Methodology flowchart

3.1. Pedestrian-Vehicle Conflict Assessment

This research employed PET as the main conflict indicator to assess the levels of conflicts involving pedestrians and vehicles. Additionally, vehicle speed, known for its strong correlation with crash risk (Zhang et al., 2015), was also considered as an SSM. PET is defined as the time difference between the first road user (pedestrian in this research) leaving the virtual conflict zone (t_1) and the second road user reaching the same conflict zone (t_2) (Varhelyi, 1998). PET is expressed as shown in Equation (1).

$$PET = t_2 - t_1 \quad (1)$$

This research focused exclusively on pairwise interactions, specifically examining interactions involving a single pedestrian and single vehicle at a time. To analyze these interactions, PET was computed, utilizing trajectories derived from the coordinates of bounding boxes of detected pedestrians and vehicles.

PETs are classified into three categories: no conflict (PET: >6s), slight conflict (>3s & ≤6s), and severe conflict (≤3s) (Zhang et al., 2020a; Zhang et al., 2020b). The PET threshold was set to 6s to determine if there was a dangerous condition for pedestrians (Formosa et al., 2020; Radwan et al., 2016). This approach allowed for granular analysis of conflicts at the individual interaction level, enhancing the research's ability to understand and predict the potential risks associated with pedestrian-vehicle conflicts.

3.2. LSTM Modeling

Due to the temporal nature of trajectory data, an LSTM neural network model, proposed by Hochreiter and Schmidhuber (1997), is used in this research. The LSTM neural network is an algorithm based on recurrent neural networks (RNNs) that addresses a common issue known as the vanishing gradient problem. Unlike traditional RNNs, which struggle to capture long-term dependencies due to diminishing gradients, LSTM networks utilize a memory cell to incorporate short-term and long-term information (Arbel, 2018). This allows the LSTM neural network model to effectively retain and utilize important contextual information for accurate predictions.

The LSTM neural network model is well-suited for capturing the inherent temporal relationships present in the trajectory data. The review of the literature revealed that this type of RNNs has a high predictive power, as demonstrated in various applications in traffic safety (Zhang et al., 2020a; Zhang et al., 2020b; Li et al., 2020; Jiang et al., 2020). By effectively modeling these temporal dependencies, the LSTM neural network model ensures optimal performance metrics, including recall, precision, F1 score, and accuracy, compared to traditional models such as the autoregressive integrated moving average (ARIMA) model.

The proposed LSTM neural network model analyzes the sequential information from the pedestrian and vehicle trajectories and captures important temporal dependencies to predict the severity levels of conflicts, considering various factors, including the vehicle direction, pedestrian gender, crossing direction, and compliance with the traffic lights.

3.2.1. LSTM Structure

The structure of an LSTM cell at each time step is depicted in Figure 2. LSTMs comprise three essential layers: an input layer, a hidden layer, and an output layer. The input and output

layers consist of conventional neurons, while the hidden layer comprises memory blocks that serve as information stores.

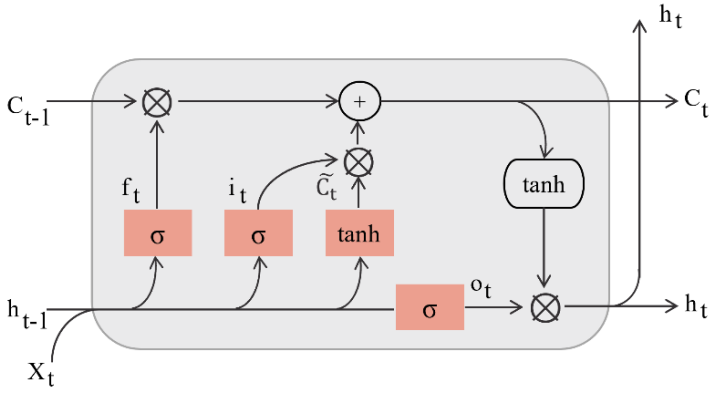

Figure 2. Structure of an LSTM cell

These memory blocks of the hidden layer contain self-connected memory cells and three multiplicative units known as gates: the input gate, output gate, and forget gate. These gates are crucial in performing continuous analogs of write, read, and reset operations on the memory cells. The computations carried out by these gates can be explained using Equations (2)-(4), which provide a mathematical representation of their functionalities.

$$i_t = \sigma\left(W_i\left[h_{t-1}, X_t\right] + b_i\right) \tag{2}$$

$$f_t = \sigma\left(W_f\left[h_{t-1}, X_t\right] + b_f\right) \tag{3}$$

$$o_t = \sigma\left(W_o\left[h_{t-1}, X_t\right] + b_o\right) \tag{4}$$

where i_t, f_t, o_t, and σ represent input gate, forget gate, output gate, and sigmoid function, respectively. W_x is the weight for the respective gate (X) neurons. h_{t-1} is the output of the previous LSTM block (at time stamp t-1). X_t is the input at current timestamp, and b_x represents biases for the respective gates (X).

The cell state (memory), candidate cell state, and the final output are given in Equations (5)-(7), respectively.

$$\tilde{C}_t = \tanh\left(W_c\left[h_{t-1}, X_t\right] + b_c\right) \tag{5}$$

$$C_t = f_t \otimes C_{t-1} + i_t \otimes \tilde{C}_t \tag{6}$$

$$h_t = o_t \otimes \tanh\left(C_t\right) \tag{7}$$

where tanh and $\otimes$ are respectively activation function tanh and elementwise product of vectors.

3.2.2. LSTM Model Development and Evaluation

Like for any other machine learning or deep learning algorithm, careful tuning of hyperparameters is necessary while developing an LSTM neural network model to enhance its predictability power. The following parameters are typically involved in the tuning process: batch size, number of LSTM units, learning rate, number of epochs, dropout rate, optimizer, and activation.

Batch size refers to the number of training examples processed simultaneously during each training iteration. The number of LSTM units corresponds to the total number of memory cells or hidden units within an LSTM layer. The learning rate determines the step size at which the LSTM model's weights are updated during training. The number of epochs refers to the number of times the entire training dataset is passed forward and backward through the LSTM network during training.

The dropout rate is a probability value that randomly deactivates units or connections during training to prevent overfitting and improve generalization. The optimizer is an algorithm

responsible for adjusting the model's parameters (weights and biases) during training to minimize errors. Activation in LSTM refers to the non-linear function applied to input and recurrent connections within the LSTM cell. It introduces non-linearity and regulates the information flow within the LSTM network.

To evaluate the training quality of the LSTM model, the area under the curve (AUC) value was used. The AUC provides a comprehensive measure of how well the model has been trained and its ability to discriminate between positive and negative samples. The performance of the LSTM neural network was assessed using various metrics, as outlined in Equations (8)-(11). Accuracy, a metric that considers both positive and negative samples, represents the ratio of correctly classified samples to the entire dataset.

Precision, also known as the positive predictive value, is the ratio of actual positive samples to classified positive samples. It provides insight into the model's ability to accurately identify positive instances. Recall, also referred to as sensitivity or true positive rate, measures the proportion of correctly classified positive samples out of the total number of actual positive samples. It indicates the model's capability to capture positive instances effectively. The F1 score is an integrated metric that considers both precision and recall. It balances these two metrics and serves as an overall indicator of the model's performance.

$$\text{Accuracy} = \frac{TP + TN}{TP + FP + FN + TN} \tag{8}$$

$$\text{Precision} = \frac{TP}{TP + FP} \tag{9}$$

$$\text{Recall} = \frac{TP}{TP + FN} \tag{10}$$

$$\text{F1 score} = \frac{2 \times \text{Precision} \times \text{Recall}}{\text{Precision} + \text{Recall}} \tag{11}$$

where TP, TN, FP, and FN are the true positive, true negative, false positive, and false negative, respectively.

3.3. Adjacent-Category Approach Modeling

In this research, the ordered logit approach is used to model the effects of variables pertaining to pedestrians, vehicles, and signal timing-related factors on the severity of pedestrian-vehicle conflicts, considering the transition from the lower level of conflict to the adjacent higher one. When comparing two categories in the ordinal outcome, i.e., conflict level is of substantive interest, the adjacent approach is the most appropriate among the ordered logistic regression models (Fullerton and Anderson, 2021).

Three adjacent approach-based models are used to model the severity of pedestrian-vehicle conflicts: the adjacent category (AC) model, the partial adjacent category (PAC) model, and the adjacent category model with partial proportionality constraints (ACPPC).

3.3.1. AC Modeling

The AC model (Goodman, 1983) requires the PO assumption. This means that no specific variable related to pedestrian, vehicle, or signal timing-related factors have a disproportionately larger effect on a particular level of pedestrian-vehicle conflict.

The AC model, as described in Equation (12), provides a mathematical representation of how this model calculates and predicts the levels of pedestrian-vehicle conflict.

$$\mathrm{Log}\left(\frac{\Pr(y=m|\mathbf{x})}{\Pr(y=m+1|\mathbf{x})}\right)=\omega_m-\mathbf{x}\boldsymbol{\beta} \qquad 1\le m<M \tag{12}$$

where m is a conflict severity level, x is a vector of pedestrian, vehicle, and signal timing variables, ω is a cut point, and β is a vector of logit coefficients.

The probability of any given conflict severity level (m) (Long and Cheng, 2004) in the AC model is given in Equation (13), with β not varying across adjacent comparisons and other parameters defined previously.

$$\Pr(y=m|\mathbf{x})=\begin{cases}\dfrac{\exp\left(\sum_{r=m}^{M-1}\left[\omega_r-\mathbf{x}\boldsymbol{\beta}\right]\right)}{1+\sum_{q=1}^{M-1}\left[\exp\left(\sum_{r=q}^{M-1}\left[\omega_r-\mathbf{x}\boldsymbol{\beta}\right]\right)\right]} & 1\le m\le M-1\\ 1-\sum_{q=1}^{M-1}\Pr(y=q|\mathbf{x}) & m=M\end{cases} \tag{13}$$

3.3.2. PAC Modeling

The PAC model is another model within the adjacent approach that relaxes the PO assumption for coefficients with a significant variation across logit equations. The probability of any given conflict severity level (m) is given in Equation (14), which is a modification of Equation (13).

$$\Pr(y=m|\mathbf{x})=\begin{cases}\dfrac{\exp\left(\sum_{r=m}^{M-1}\left[\omega_r-\mathbf{x}_1\boldsymbol{\beta}_{1r}-\mathbf{x}_2\boldsymbol{\beta}_2\right]\right)}{1+\sum_{q=1}^{M-1}\left[\exp\left(\sum_{r=q}^{M-1}\left[\omega_r-\mathbf{x}_1\boldsymbol{\beta}_{1r}-\mathbf{x}_2\boldsymbol{\beta}_2\right]\right)\right]} & 1\le m\le M-1\\ 1-\sum_{q=1}^{M-1}\Pr(y=q|\mathbf{x}) & m=M\end{cases} \tag{14}$$

where ω is a cut point, x_1 and x_2 are vectors of pedestrian, vehicle, and signal timing variables, β_1 is a vector of logit coefficients allowed to vary across equations, and β_2 is a vector of logit coefficients constrained to be equal across equations.

3.3.3. ACPPC Modeling

The third model used in this research is the ACPPC model (Anderson, 1984). Unlike the PAC model, which allows certain coefficients to vary freely across equations, the ACPPC model relaxes the PO assumption by constraining all or some coefficients to vary by a common factor φ. Modifying Equation (13) yields the following Equation (15) for the probability of any given conflict severity level (m) in the ACPPC model.

$$\Pr(y=m|\mathbf{x})=\begin{cases}\dfrac{\exp\left(\sum_{r=m}^{M-1}\left[\omega_r-\mathbf{x_1}\varphi_r\boldsymbol{\beta_1}-\mathbf{x_2}\boldsymbol{\beta}_{2r}-\mathbf{x_3}\boldsymbol{\beta_3}\right]\right)}{1+\sum_{q=1}^{M-1}\left[\exp\left(\sum_{r=q}^{M-1}\left[\omega_r-\mathbf{x_1}\varphi_r\boldsymbol{\beta_1}-\mathbf{x_2}\boldsymbol{\beta_{2r}}-\mathbf{x_3}\boldsymbol{\beta_3}\right]\right)\right]} & 1\le m\le M-1\\ 1-\sum_{q=1}^{M-1}\Pr(y=q|\mathbf{x}) & m=M\end{cases} \quad (15)$$

where ω is a cut point, x_1, x_2, and x_3 are vectors of pedestrian, vehicle, and signal timing variables, β_1 is a vector of logit coefficients that vary by a common factor φ across equations, β_2 is a vector of logit coefficients that vary freely across equations, β_3 is a vector of logit coefficients that do not vary across equations, and m is the logit equation.

The three models are compared. Once the best-fitting model is determined, the interpretation involved analyzing the estimated coefficients or weights associated with the variables in the model.

CHAPTER 4: DATA COLLECTION AND PROCESSING

4.1. Data Collection

Two specific locations in Concord, NC, United States, were selected to assess and model pedestrian-vehicle conflicts. The first location is a signalized crosswalk at the Cabarrus Ave & Union St intersection (35.4105695° & -80.5813986°). The second intersection is a crosswalk with an RRFB located at the Cabarrus Ave & Market St intersection (35.410031° & -80.582056°).

The two locations were selected due to the observation of many pedestrians ignoring traffic lights and jaywalking, and the configuration of the roads or their surroundings. Details of the two crosswalks are shown in Figure 3 and Figure 4. The trap length of 110 feet (33.5 m) in the longitudinal direction of the road was found adequate to observe the road environment and vehicle and pedestrian trajectories in the vicinity of the crosswalk. In addition, this length corresponds approximately to the driver stopping sight distance.

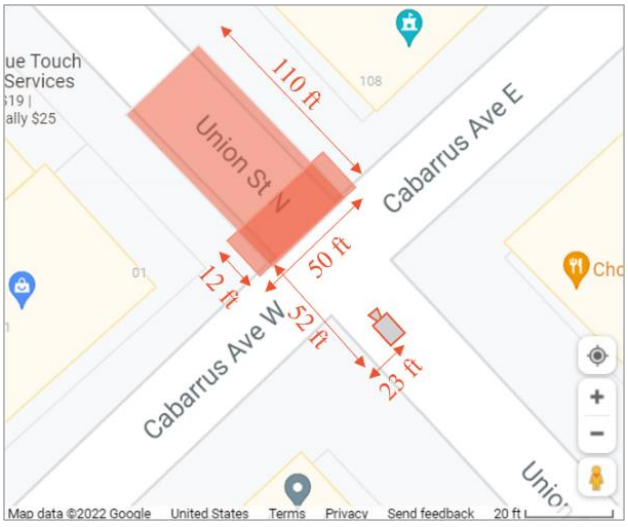

Figure 3. Cabarrus Ave & Union St crosswalk location © 2022 Google Maps

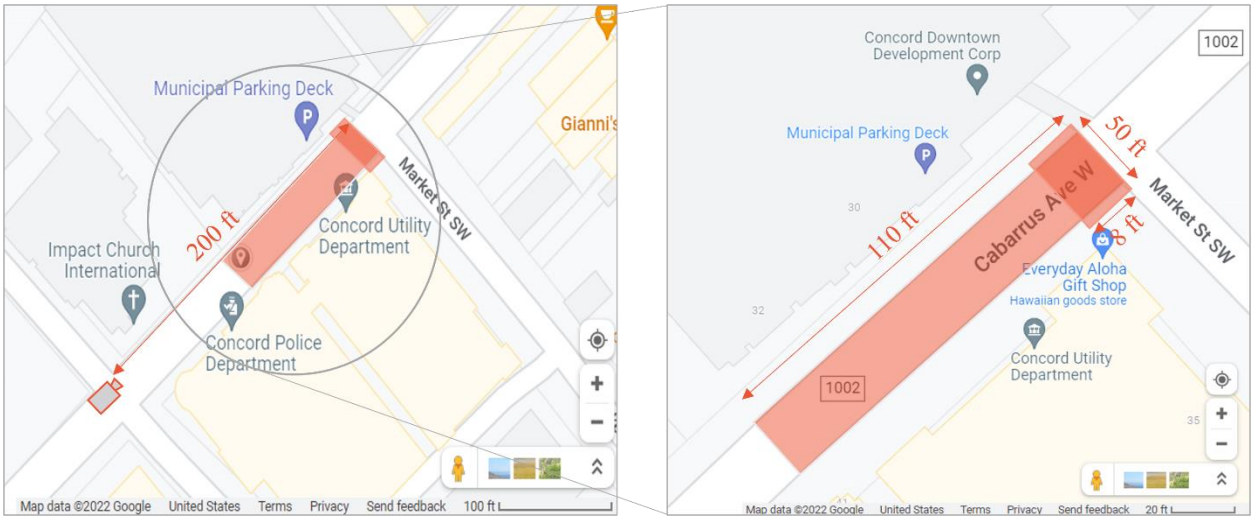

Figure 4. Cabarrus Ave & Market St crosswalk location © 2022 Google Maps

The speed limits on Union St N and Cabarrus Ave W are 25 mph and 20 mph, respectively. The fixed-cycle intersection operates in two phases during its traffic cycle, which lasts for 60s. Vehicles experience a 35-second green time, followed by a 5-second yellow time, and finally, a 20-second red time along the approach used in this study. The RRFB system at the second location flashes yellow for 5 seconds once a pedestrian has engaged it. This flashing yellow signal alerts drivers to exercise caution and be aware of pedestrians' presence at the crosswalk.

The video data obtained from the city of Concord, North Carolina was recorded at each location on March 25 and 26, 2021. The data consisted of 12 hours of recorded videos (7:00 a.m. to 7:00 p.m.) for each day sizing approximately 9.5 GB with a resolution of 1920×1080 pixels and a frame rate of 30 frames per second (FPS). Consequently, the data collection involved detecting and tracking pedestrians and vehicles who entered the highlighted zones in Figure 3 and Figure 4, considering the travel directions of vehicles (V1, V2, and V3), the crossing directions of regular pedestrians (P1 and P2), and those of jaywalkers (J1 and J2) as shown in Figure 5 and Figure 6.

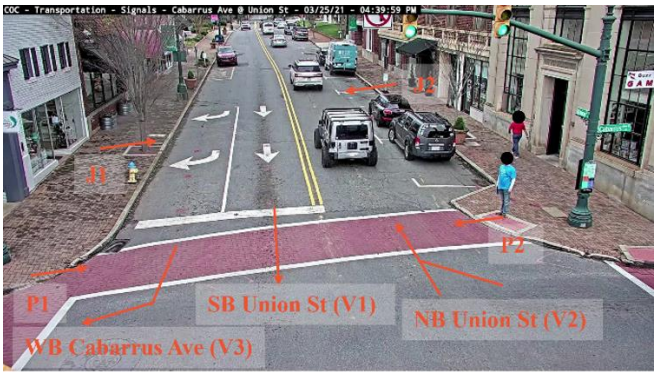

Figure 5. Illustration of vehicle and pedestrian directions at the fixed-cycle intersection

Figure 6. Illustration of vehicle and pedestrian directions at the RRFB-controlled intersection

4.2. Data Extraction and Processing

This research employed the tracking-by-detection approach with YOLOv4 (Bochkovskiy et al., 2020) for detection and DeepSORT (Wojke et al., 2017) for tracking.

YOLOv4 is applied to video data as it offers a better ratio of speed to accuracy (Chahal and Dey, 2018). DeepSORT is used for tracking purposes due to its capability to find a previously tracked object (person or vehicle) even if it has been occluded (Wojke et al., 2017). Therefore, the tracking-by-detection approach used pre-trained object detection (Bochkovsky, 2020) and object tracking (Wojke, 2017) algorithms.

4.2.1. Traffic Flow Extraction

YOLOv4, a highly effective object detection algorithm, has demonstrated its capabilities on the widely used common object in context (COCO) dataset (Lin et al., 2014). Its performance was evaluated based on the rigorous standards of the MOT16 Challenge benchmark (Milan et al., 2016), which specifically measures the effectiveness of MOT algorithms.

In prior research, YOLOv3 was employed for detecting road users in traffic video data (Zhang et al., 2020a; Zhang et al., 2020b; Jana et al., 2018; Lin and Sun, 2018). Concurrently, DeepSORT, another prominent tracking algorithm, has numerous applications in transportation (Zhang et al., 2020a; Zhang et al., 2020b; Arvind et al., 2019; Hou et al., 2019).

Figure 7 illustrates the steps in the data extraction process using the proposed tracking-by-detection approach.

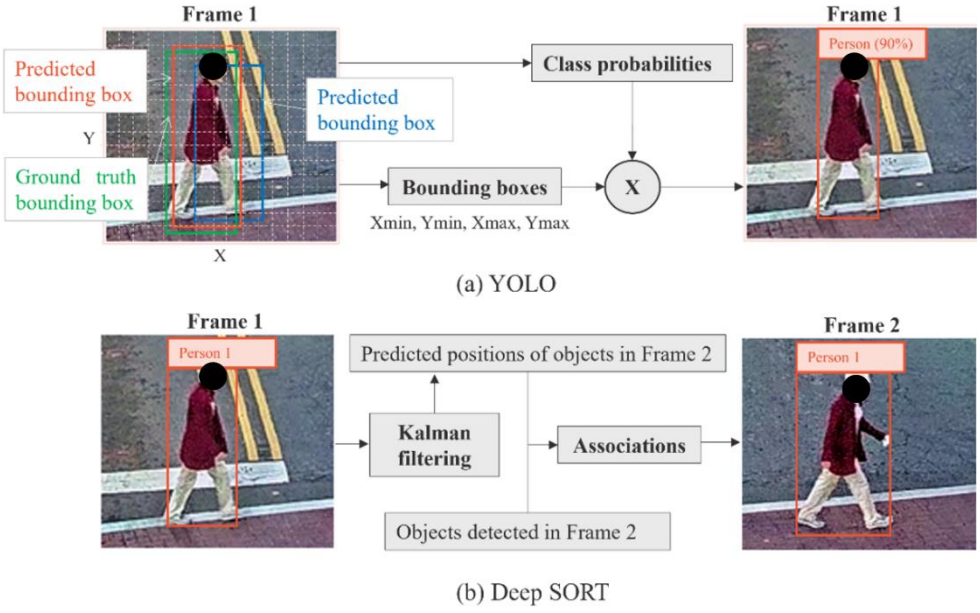

Figure 7. Steps in the data extraction process

The initial step involves dividing Frame 1 into a grid of size S×S (typically 19×19) for the prediction of C object class (such as pedestrian or vehicle) probabilities and B bounding boxes (typically 5), each accompanied by a confidence score. Equation (16) illustrates the process of merging the class probabilities and bounding boxes into a unified score.

$$\Pr(\text{Class}_i|\text{Object}) \times \Pr(\text{Object}) \times \text{IoU}_{\text{gt,pred}} = \Pr(\text{Class}_i,\text{Object}) \times \text{IoU}_{\text{gt,pred}} \quad (16)$$

where $\Pr(\text{Class}_i \mid \text{Object})$ is the predicted conditional probability that the object belongs to class i given the presence of an object, Pr(Object) is the predicted probability that the bounding box contains an object, $\text{IoU}_{\text{gt, pred}}$ is the estimated Intersection over Union (IoU) between the predicted box and a ground truth box, and $\Pr(\text{Class}_i, \text{Object})$ is the predicted probability that the object belongs to Class_i.

The detections of pedestrians and vehicles were filtered based on a confidence score threshold of 0.5, which is typically the minimum acceptable threshold. The motion information was estimated using a Kalman filter, which helped in tracking the objects over time.

To maintain the identities of pedestrians and vehicles, their feature embeddings were tracked and associated across frames using the Hungarian algorithm. This association process ensured that the same object detected in consecutive frames was assigned the correct identity. True positives were determined based on a minimum overlap of 50% with the corresponding ground truth bounding box. This criterion ensured that the tracked objects were considered true positives when they sufficiently overlapped with the ground truth annotations.

4.2.2. Speed Estimation

In the data extraction phase, the positions of vehicles and pedestrians were recorded over time, frame by frame, using the middle bottom point on the bounding box. Equation (17) expresses the instantaneous speeds for individual pedestrians and vehicles. Equation (18) expresses the crossing speed calculated by averaging instantaneous speeds. Afterward, the average crossing speed was computed using Equation (19). These equations were proposed by Fu et al. (2016) and are based on Figure 8, which illustrates the details of the computation of vehicle speeds. The same procedure is applicable for pedestrian crossing speeds.

$$v_{i,j,k} = \frac{x_{j,k} - x_{j,k-1}}{t_{j,k} - t_{j,k-1}} \tag{17}$$

$$v_{i,j} = \frac{1}{1 - f + 1} \sum_{k=f}^{l} \left(v_{i,j,k} \right) \tag{18}$$

$$v_a = \frac{1}{q} \sum_{j=1}^{q} \left(v_{i,j} \right) \tag{19}$$

where j, j =(1,…,q) represents a pedestrian or vehicle, x is its x-coordinates at frames k and k-1 that falls within the defined crosswalk zone as shown in Figure 8, t refers to the related instants of its detections, v_a is the average crossing speed of pedestrians or vehicles depending on the side I of the crosswalk, or the direction they are traveling, and f and l stand for the first and last frames that fall within the conflict zone.

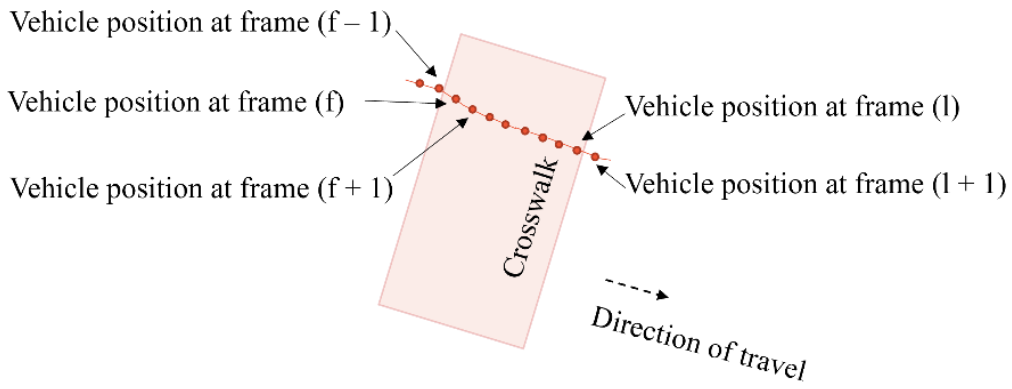

Figure 8. Illustration of vehicle speed estimation

4.2.3. Speed and Trajectory Validation

To validate the extracted data, a comprehensive evaluation was conducted from microscopic and macroscopic perspectives. The validation process involved comparing the automatically extracted data with manually measured data.

From a microscopic perspective, individual trajectories of pedestrians and vehicles were compared between the automated extraction and manual measurements. This comparison aimed to assess the accuracy of the generated trajectories. From a macroscopic perspective, the average speeds of pedestrians and vehicles were compared between the automated extraction and manual measurements. This comparison provided insights into the accuracy of the computed speeds.

Kinovea software (Charmant et al., 2021), a semi-automated tracking software, was used for validation. This software enables precise angular and linear measurements by digitizing x- and y-axis coordinates (Kathuria et al., 2020). Consequently, it is considered a reliable tool for extracting traffic data, including trajectories and speeds (Chen et al., 2022; Karimi et al., 2021; Kathuria et al., 2020).

In addition to R-squared representing the precision of the software, mean relative error (MRE), relative precision error (RPE), and relative accuracy error (RAE) are used in the current

literature for validation (Kathuria et al., 2020; Fu et al., 2017). Therefore, the same metrics, as expressed in Equation (20)-(22), were used in this research.

$$\mathrm{MRE} = \frac{1}{100} \sum \frac{\left| V_a - V_m \right|}{V_m} \tag{20}$$

$$\mathrm{RPE} = \frac{1}{100} \sum \frac{\left| \left(V_a - y_{intercept} \right) - V_m \right|}{V_m} \tag{21}$$

$$\mathrm{RAE} = \frac{1}{100} \sum \frac{\left| y_{intercept} \right|}{V_m} \tag{22}$$

where V_a and V_m are the automatically extracted and manually measured speeds, and $y_{intercept}$ represents the speed value when the fitted line crosses the y-axis ($V_m = 0$).

CHAPTER 5: ASSESSING PEDESTRIAN-VEHICLE CONFLICTS

This chapter focuses on assessing pedestrian safety based on the severity of pedestrian-vehicle conflicts. The tracking-by-detection approach was used to extract traffic data and compute pedestrian speeds, vehicle speeds, and PETs. Afterward, macroscopic and microscopic validation was conducted. The analysis further examined the proportion of jaywalkers and its association with vehicular traffic volume and the proportion of pedestrian red-light violations.

5.1. Pedestrian Safety Assessment at the Fixed-Cycle Intersection

This section is dedicated to the pedestrian safety assessment for the Cabarrus Ave & Union St intersection. This safety assessment focused on identifying pedestrian-vehicle conflicts and their severities using PETs. Trajectories and speeds of pedestrians and vehicles were extracted and validated before assessing pedestrian-vehicle conflicts.

5.1.1. Vehicular and Pedestrian Volumes at the Fixed-Cycle Intersection

The vehicular and pedestrian volumes were estimated using the tracking-by-detection approach. Figure 9 illustrates detected and tracked pedestrians and vehicles in the crosswalk zone. Pedestrians and vehicles were identified through bounding boxes as person and car, respectively. They were assigned unique IDs. The tracking-by-detection system counted pedestrians and vehicles on a frame-by-frame basis and created a spreadsheet that included frame numbers, IDs of detected pedestrians and vehicles, the four coordinates of their bounding boxes, and the times of detection. The values of these coordinates are defined in pixels based on the scale of the video

frame (1920×1080 pixels). Only pedestrians and vehicles with consistent IDs in the highlighted zone depicted in Figure 3 were considered for further analysis.

Figure 9. Illustration of detected and tracked pedestrians and vehicles at the fixed-cycle intersection

The results regarding the temporal variability of traffic by direction, including vehicular and pedestrian volumes, are presented in Table 1. The video data recorded on March 25 and 26, 2023 was aggregated. The directions of pedestrians and vehicles, as depicted in Figure 5, were identified by tracking the coordinates of bounding boxes.

Table 1 provides an overview of the traffic volumes, indicating a generally stable distribution, as none of the proportions exceed 50% for any time of the day. Nevertheless, there is a noticeable pattern of increased pedestrian and vehicular volumes during the afternoon hours compared with the morning hours.

Table 1. Variability of vehicular and pedestrian volumes at the fixed-cycle intersection

Time of the day (TD)	Vehicle direction			Pedestrian direction			
	V1	V2	V3	P1	P2	J1	J2
07:00 a.m. - 09:00 a.m. (TD1)	216 (6.10%)	422 (13.10%)	102 (10.40%)	24 (7.90%)	22 (7.20%)	14 (14.60%)	6 (15.00%)
09:00 a.m. - 11:00 a.m. (TD2)	330 (9.30%)	414 (12.80%)	94 (9.60%)	26 (8.60%)	40 (13.10%)	11 (11.50%)	4 (10.00%)
11:00 a.m. - 01:00 p.m. (TD3)	508 (14.40%)	564 (17.50%)	196 (20.00%	72 (23.80%)	56 (18.30%)	16 (16.70%)	4 (10.00%)
01:00 p.m. - 03:00 p.m. (TD4)	870 (24.60%)	618 (19.10%)	182 (18.50%)	66 (21.90%)	58 (19.00%)	18 (18.80%)	12 (30.00%)
03:00 p.m. - 05:00 p.m. (TD5)	772 (21.80%)	694 (21.50%)	190 (19.30%)	64 (21.20%)	62 (20.30%)	25 (26.00%)	8 (20.00%)
05:00 p.m. - 07:00 p.m. (TD6)	844 (23.80%)	516 (16.00%)	218 (22.20%)	50 (16.60%)	68 (22.20%)	12 (12.50%)	6 (15.00%)
Total per direction (TD1-TD6)	3540	3228	982	302	306	96	40
Total (all directions)	7750			608		136	

Note: V1, V2, and V3 are vehicle directions, and P1 (J1) and P2 (J2) are regular pedestrian (jaywalker) crossing directions, as indicated in Figure 5. Values in parentheses represent the proportions of traffic volumes.

5.1.2. Pedestrian and Vehicle Trajectories at the Fixed-Cycle Intersection

Figure 10 and Figure 11 present snapshots of pedestrian and vehicle trajectories. The reference point used to locate pedestrians and vehicles was the middle bottom point of bounding boxes. Zhang et al. (2021b) also use the same reference to locate pedestrians and predict their crossing intentions. The trajectories were generated by tracking movements of pedestrians and vehicles across consecutive frames over time.

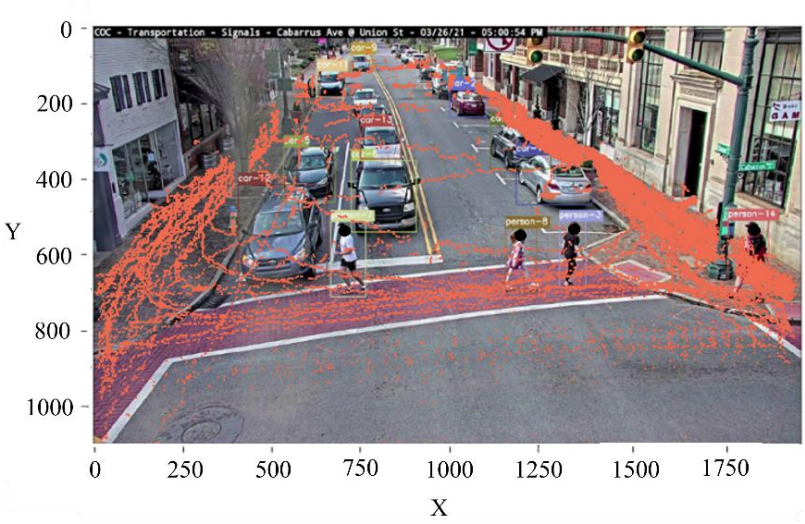

Figure 10. Snapshot of pedestrian trajectories at the fixed-cycle intersection

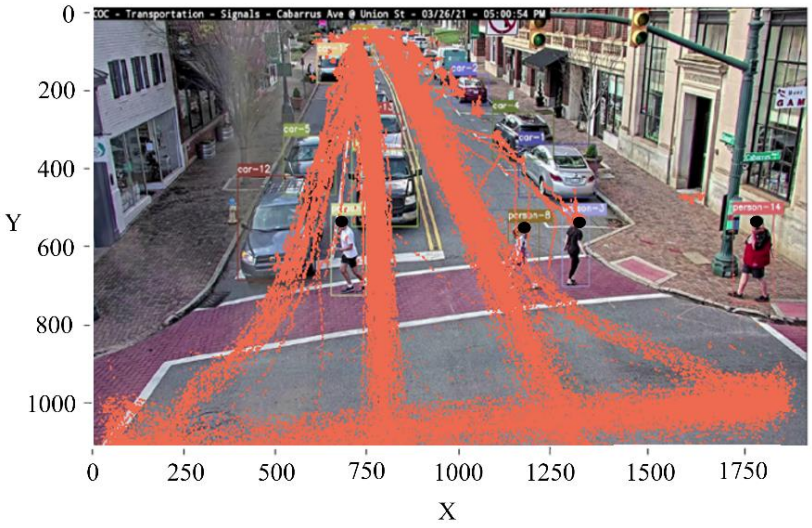

Figure 11. Snapshot of vehicle trajectories at the fixed-cycle intersection

Figure 10 shows that, despite the presence of a designated crosswalk, instances of jaywalking still occur. This phenomenon can be attributed to several factors. Firstly, the compact nature of the intersection and its relatively narrow lane widths may make it more convenient for pedestrians to directly cross the road from the sidewalk instead of waiting at the curb for the pedestrian green phase. Additionally, the presence of the parking lane can obstruct the visibility of

oncoming drivers, making it difficult for them to spot jaywalkers and posing a substantial risk to pedestrian safety. The pedestrian trajectories depicted in Figure 10 highlight the potential issue with the design of the crosswalk, a lack of enforcement of traffic laws and inadequate education and awareness campaigns for pedestrians. Furthermore, some pedestrians may have disregarded the traffic lights although they crossed using the crosswalk (Zhou et al., 2013). This situation necessitates further investigation to assess the safety of pedestrians during their interactions with vehicles and to predict the potential severity of conflicts that could lead to more serious incidents like crashes.

5.1.3. Average Pedestrian and Vehicle Crossing Speeds at the Fixed-Cycle Intersection

5.1.3.1. Average pedestrian crossing speeds at the fixed cycle intersection

The results of the two-way ANOVA reveal that the average pedestrian crossing speeds are tributary of the time of the day and not the direction of crossing. The F-statistic for travel direction is 0.05 with a corresponding p-value of 0.823, indicating that it is not statistically significant. On the other hand, the F-statistic for the time of day is 13.75 with a p-value of less than 0.01, suggesting that it significantly impacts pedestrian crossing speeds.

Figure 12 reveals no substantial difference in average pedestrian crossing speeds across different times of the day. This lack of clear patterns can be attributed to the unpredictability and inconsistency of pedestrian patterns, as depicted in Figure 10. Unlike drivers, pedestrians have more varying behaviors and preferences using the road space.

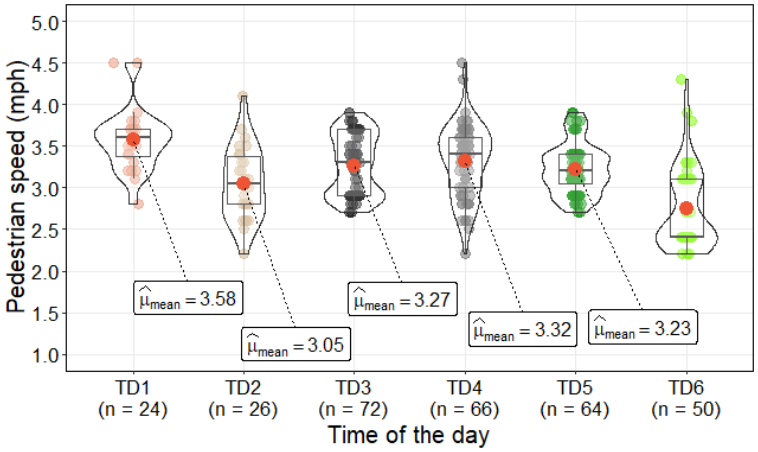

(a) P1 direction

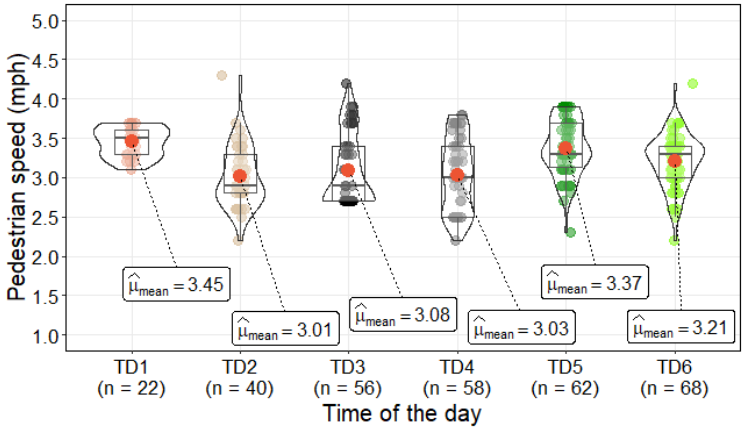

(b) P2 direction

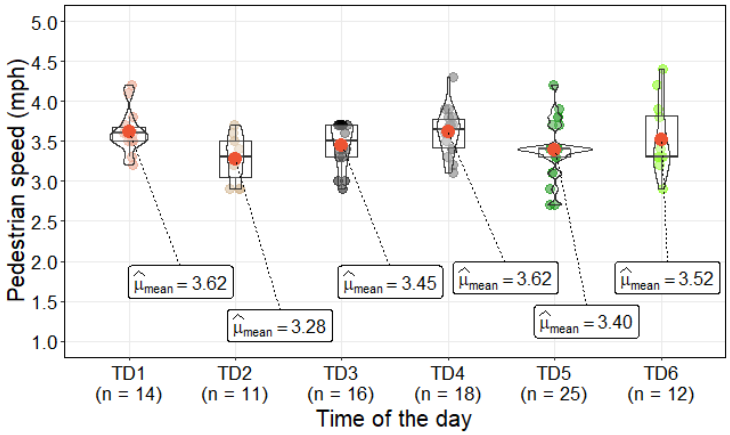

(c) J1 direction

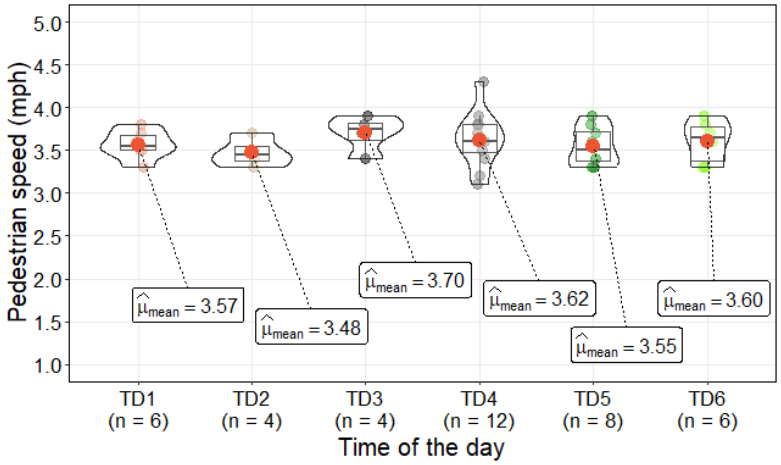

(d) J2 direction

Figure 12. Average pedestrian speeds at the fixed-cycle intersection by time of the day and crossing direction

Figure 12 also shows that jaywalkers cross the road at a faster pace compared with regular pedestrians. This behavior can be attributed to their desire to minimize their exposure to potential conflicts with vehicles, as they are aware of violating traffic rules by not using the designated crosswalk (Zhou et al., 2013). The highest crossing speed for both regular pedestrians and jaywalkers is 4.5 mph.

5.1.3.2. Average vehicle speeds at the fixed-cycle intersection

Estimating vehicle speeds is crucial as it indicates the potential safety risks drivers may pose to pedestrians. Therefore, gathering data on vehicle speeds is essential to identify potential safety hazards. Figure 13 shows the average vehicle speeds throughout the day, categorized by their respective directions of travel. This figure illustrates the patterns of vehicle speed variation over time.

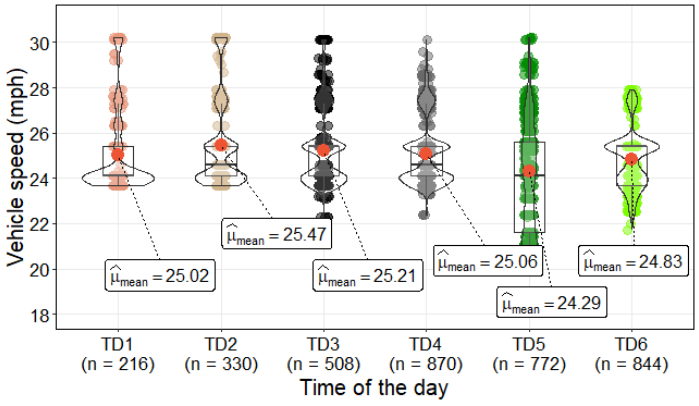

(a) V1 direction

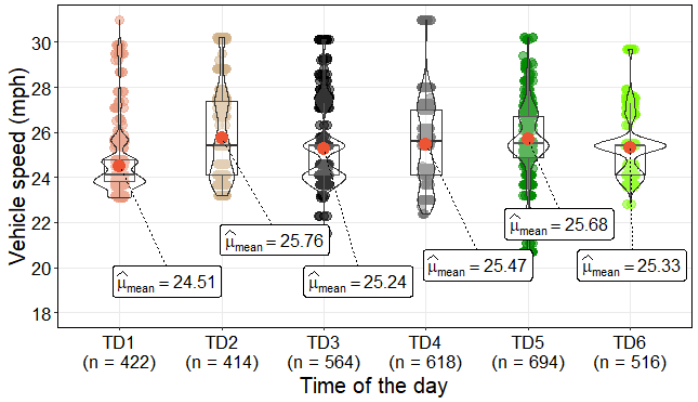

(b) V2 direction

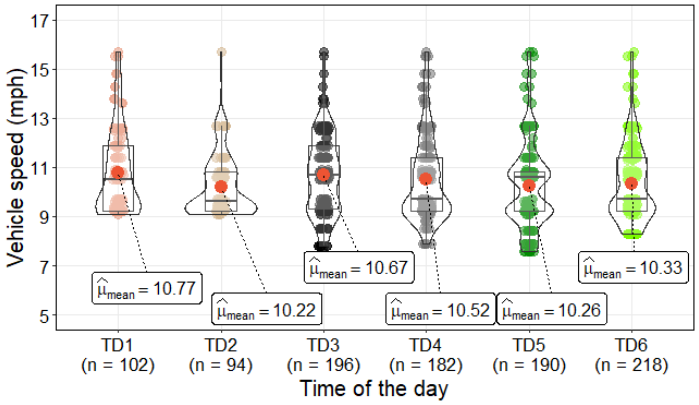

(c) V3 direction

Figure 13. Average vehicle speeds at the fixed-cycle intersection by time of the day and travel direction

It is important to note that the average vehicle speeds shown in Figure 13 (a)-(c) were specifically computed for the allocated green phase, representing the period during which vehicles have the ROW to proceed through the intersection. According to the results in Figure 13(a) and Figure 13(b), the maximum average speeds recorded for vehicles in the V1 and V2 directions was 31.7 mph. Similarly, the highest average speed for vehicles in the V3 direction was 15.7 mph (Figure 13(c)).

Based on Figure 13, the mean of all average speeds aligns closely with the 25-mph speed limit, indicating a quasi-compliance with the set limit. Further statistical analysis was conducted using a two-way ANOVA to explore the influence of travel direction and time of the day on average vehicle speeds. The results indicated that the direction of travel and time of the significantly impact average vehicle speeds. The F-statistic values of 27096.6 for travel direction and 57.2 for time of the day, along with their corresponding p-values below 0.01, validate this finding. However, when conducting pairwise comparisons using the Tukey test, not all differences in average speeds between different times of the day were significant. Specifically, significant differences in average speeds were observed for the V1 direction before and after 1:00 PM (TD1, TD2, and TD3). In contrast, significant differences in average vehicle speeds were observed only between TD1, TD2, and TD3 for the V2 direction, while no significant differences were found for other times of the day.

The significance of the statistical difference in average crossing speeds among drivers highlights the unpredictability and heterogeneity of drivers' behavior. A total of 3518 drivers exhibited speeds higher than the 25-mph speed limit, indicating the necessity of conducting a microscopic safety assessment to evaluate the potential risks individual drivers may pose to pedestrians. This heterogeneity in vehicle speeds can be attributed to the diverse behaviors

exhibited by drivers. Past research revealed that drivers behave differently when approaching signalized intersections (Singh et al., 2022). For example, some drivers may perceive the red light or the length of the vehicle queue as too long, prompting them to attempt to pass through the intersection faster than they are supposed to (Wu et al., 2019).

The speed data analysis for the V3 direction indicated no significant differences in average speeds observed across different times of the day. This can be observed in Figure 13(c), where vehicles in this lane maintained a relatively consistent speed throughout the day. One possible explanation for this consistency in speeds is that drivers on this lane may exercise caution due to the presence of a right turn and the potential for pedestrians heading toward the crosswalk. This cautious approach may contribute to a more regulated and consistent traffic flow, resulting in less variability in average speeds over time (Fu et al., 2019).

5.1.4. Macroscopic and Microscopic Validation for the Fixed-Cycle Intersection

The video calibration was performed using the Kinovea software, exploring its built-in perspective grid, as illustrated in Figure 14. The longitudinal and transversal dimensions of the zone of interest were incorporated into the calibration plane. A grid with dimensions of 15x15 was found appropriate for accurate calibration.

Each point on the grid was then subjected to a conversion operation that transformed its pixel-based coordinates into real-world coordinates, allowing for accurate mapping of the video frame to the physical environment. Subsequently, manual tracking of pedestrians and vehicles was conducted frame by frame using the calibrated video. The number of frames analyzed in the Kinovea software corresponded to those used in the automated tracking-by-detection approach, specifically for sections of the video selected for validation purposes.

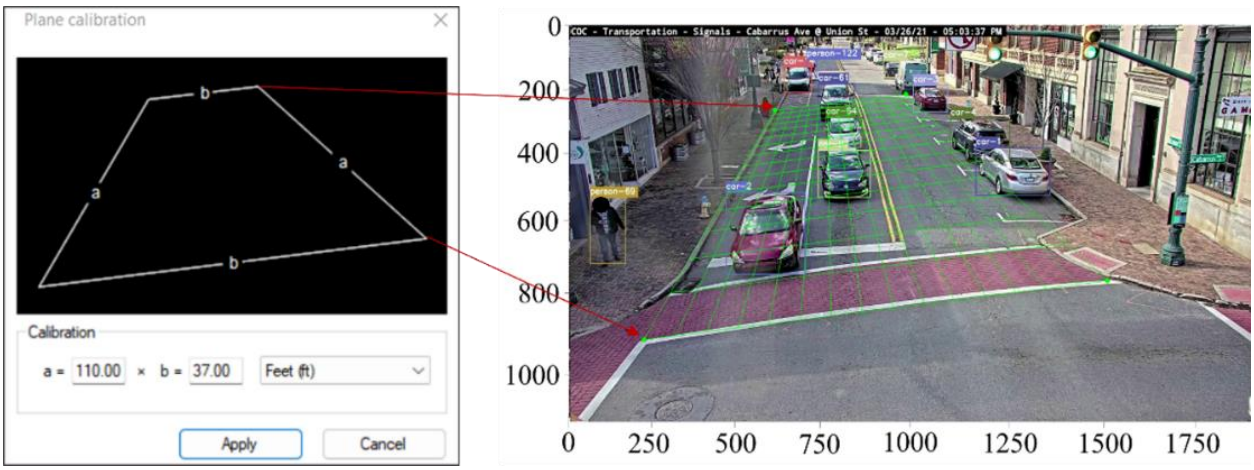

Figure 14. Grid overlaid over a video frame of the fixed-cycle intersection

5.1.4.1. Pedestrian and vehicle speed validation

The macroscopic validation procedure involved comparing the automatically extracted speeds with the manually measured speeds. Figure 15 and Figure 16 show the correlation between the automatically extracted and the manually measured speeds for pedestrians and vehicles, respectively.

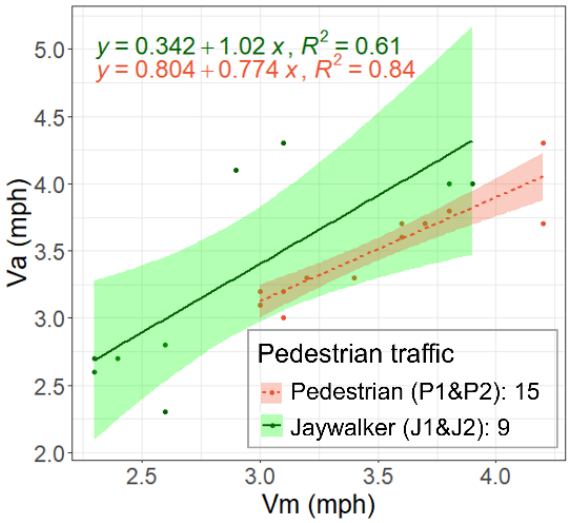

Figure 15. Pedestrian speed validation for the fixed-cycle intersection

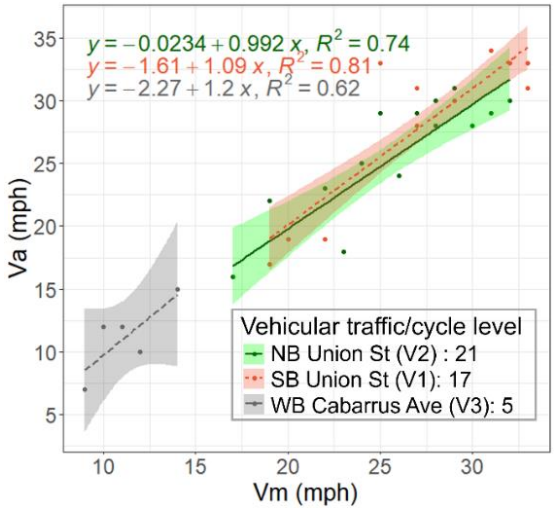

Figure 16. Vehicle speed validation for the fixed-cycle intersection

The validation for average vehicle and pedestrian speeds was performed at the signal phase level, using the maximum count of vehicles per direction. This ensured that the analysis considered the most representative data for each traffic cycle. The maximum count of pedestrians crossing the road was considered for computing the average pedestrian crossing speeds, regardless of their crossing direction. This approach was adopted due to the limited sample size and the need to include the highest number possible of pedestrians. For validating jaywalker speeds, the maximum count of jaywalkers within a 2-hour interval was considered.

Figure 15 shows that the R-squared value is considerably lower for jaywalkers than regular pedestrians. This indicates that the computed jaywalker speeds based on the extracted data might be less accurate than the speeds of regular pedestrians. It could be attributed to jaywalkers not following consistent patterns and exhibiting more variability in their crossing behaviors.

Figure 16 indicates that the R-squared values for the three vehicle directions are acceptable. However, the R-squared value is lower for the V2 direction compared to the other two directions.

This discrepancy in the R-squared values could be attributed to vehicles in the V3 lane gradually changing their direction from moving straight to making a right turn.

Table 2 provides additional validation metrics for the average speeds of pedestrians and vehicles. This table includes MRE, RPE, and RAE values for examining the accuracy and reliability of the speed predictions obtained from the data analysis. Overall, the computed average speeds for both vehicles and pedestrians are reliable.

Table 2. Validation metrics of average speeds for the fixed-cycle intersection

Metric	Vehicles			Regular pedestrians	Jaywalkers
	Northbound Union St	Southbound Union St	Westbound Cabarrus Ave		
R-square (%)	74.3	80.9	62.3	84.4	60.9
MRE (%)	3.5	4.3	8.7	5.5	11.7
RPE (%)	4.7	4.9	9.1	4.9	9.8
RAE (%)	2.3	3.7	7.4	3.2	9.1

5.1.4.2. Accuracy of pedestrian and vehicle trajectories

The Shapiro-Wilk normality test was performed on the longitudinal and transversal trajectories of both vehicles and pedestrians. The results from Table 3 demonstrate that the distribution of points for these trajectories did not significantly deviate from a normal distribution, as indicated by the p-values greater than 0.05.

Table 3. Results about microscopic validation for the fixed-cycle intersection

Road user direction	Longitudinal trajectory		Transversal trajectory	
	Shapiro-Wilk normality test	Paired sample t-test	Shapiro-Wilk normality test	Paired sample t-test
Vehicle direction				
V2	0.32	0.48	0.63	0.11
V1	0.18	0.09	0.19	0.08
V3	0.09	0.28	0.07	0.44
Pedestrian direction				
P1 and P2	0.51	0.7	0.4	0.06
J1 and J2	0.08	0.41	0.21	0.36

5.1.5. Pedestrian-Vehicle Conflicts at the Signalized Intersection

The PET was used to assess pedestrian-vehicle conflicts. It is a valuable metric for measuring near-miss situations and, consequently, the severity level of pedestrian-vehicle conflicts (Zhang et al., 2020a).

Figure 17 illustrates the distribution of PETs based on the level of conflict severity. Out of the observed 744 pedestrians, 238 pedestrians were involved in conflicts with vehicles, indicated by PET values of less than 6 seconds. Among these traffic conflicts, 55 instances involved jaywalkers, accounting for approximately 49% of the total number of pedestrians who crossed the road. It is noteworthy that the Cabarrus Ave & Union St intersection experienced a higher number of conflicts between regular pedestrians and vehicles compared to conflicts involving jaywalkers. However, only about 30% of pedestrians were involved in conflicts of slight or severe severity levels with vehicles when considering the percentage breakdown.

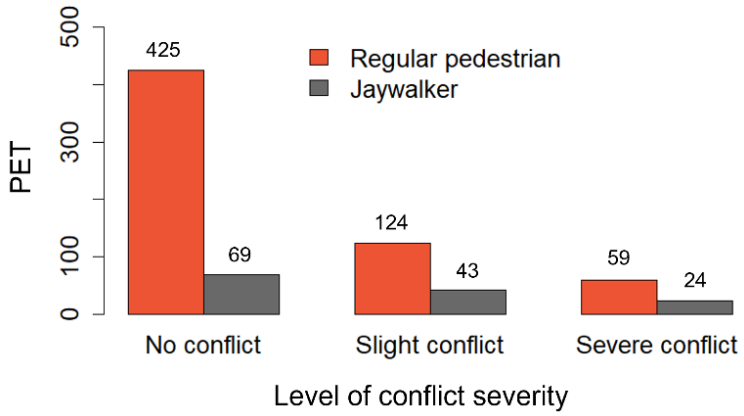

Figure 17. Distribution of PETs by type of pedestrian and level of conflict severity for the fixed-cycle intersection

Further analysis of the data indicated that among all instances of severe conflicts involving regular pedestrians, approximately 56.6% of them were found to have committed red-light violations. These findings align with previous studies (Zhang et al., 2020a; Zaki et al., 2014; Hussein et al., 2015; Zhou et al., 2013) that have also identified a positive correlation between the number and severity of conflicts and the occurrence of jaywalking and red-light violations.

The safety analysis also revealed that 92.4% of the identified jaywalkers are male pedestrians, while 82.1% of the regular pedestrians were also male. This observation aligns with previous research consistently demonstrating that male pedestrians tend to violate traffic rules more frequently than female pedestrians (Hashemi et al., 2022; Granié, 2007; Holland and Hill, 2007; Rosenbloom et al., 2004). Moreover, depending on the direction of travel of oncoming vehicles, the level of risk may vary for a pedestrian crossing in either direction. This highlights the importance of considering pedestrian crossing direction when assessing pedestrian-vehicle conflicts. Understanding the specific dynamics of each crossing direction can provide valuable insights into the potential risks and help inform targeted safety measures.

Furthermore, the research findings demonstrated that traffic violations by pedestrians tend to decrease as vehicular traffic volume increased throughout different times of the day, as depicted in Figure 18. This observation is consistent with the findings of Afshari et al. (2021), who highlighted that external factors such as traffic conditions and intersection geometry can influence pedestrian violations at intersections. The presence of adjacent parking lanes and the compact nature of the Union St & Cabarrus Ave intersection likely contributes to jaywalking or disregarding traffic lights by some pedestrians. This observation is supported by of Diependaele (2009), Duduta et al. (2014), and Yang and Sun (2013) who have reported that pedestrians are less likely to commit violations in longer crosswalks.

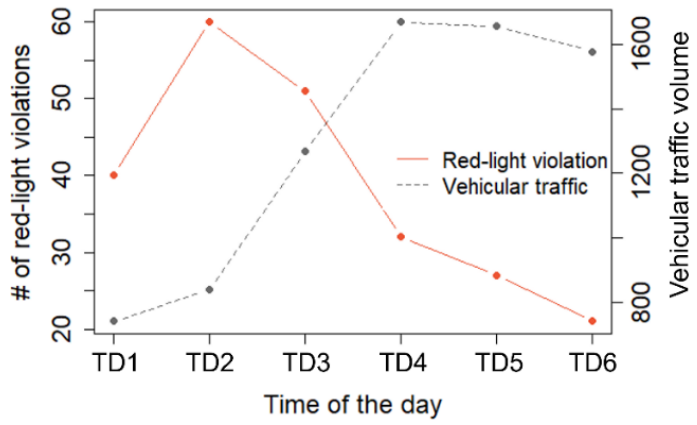

Figure 18. Pedestrian red-light violations and vehicular traffic volume by time of the day for the fixed-cycle intersection

Longer crosswalks provide pedestrians with more visible and predictable paths for crossing, reducing the incentive to engage in risky behaviors. It is important to note that approximately 90% of jaywalkers in the study crossed the road against the red light. Additionally,

jaywalkers accounted for about 53% of all observed red-light pedestrian violations, with the remaining 47% involving regular pedestrians.

Vehicle speed serves as another important measure of traffic exposure. As depicted in Figure 13, the average speeds on the northbound and southbound Union St align with the 25-mph legal speed limit for this road segment. However, it is concerning to note that out of the 7,750 vehicles counted, as deduced from Table 1, approximately 45% (3,518 vehicles) exceeded the speed limit, thereby increasing the risk to pedestrians, particularly jaywalkers and regular pedestrians who disregard traffic lights. The higher the speed, the lower the PET value and, therefore, the higher the likelihood of a crash. This finding aligns with the research conducted by Chaudhari et al. (2021) and Rosén and Sander (2009), who established a strong correlation between vehicle speed and the risk of pedestrian fatalities.

5.2. Pedestrian Safety Assessment at the RRFB-controlled intersection

The primary focus of this section is to assess pedestrian safety at the intersection of Cabarrus Ave and Market St, where an RRFB system is installed for traffic control. This safety assessment involved identifying and categorizing pedestrian-vehicle conflicts based on their severity using PETs. The extracted trajectories and speeds of pedestrians and vehicles were validated before conducting this assessment.

5.2.1. Vehicular and Pedestrian Volumes at the RRBF-Controlled Intersection

Vehicular and pedestrian volumes were estimated by counting pedestrians and vehicles with consistent identities in the crosswalk zone, as defined in Figure 4. Figure 19 illustrates detected pedestrians and vehicles through bounding boxes. These bounding boxes have four

coordinates whose values are based on the scale of a video frame. The tracking-by-detection task generated a spreadsheet containing the frame numbers, IDs of detected pedestrians and vehicles, the four coordinates of bounding boxes, and the times of detection.

Figure 19. Illustration of detected and tracked pedestrians and vehicles at the RRFB-controlled intersection

Table 4 provides the temporal variations of traffic in different directions, encompassing both vehicular and pedestrian volumes. Table 4 presents the aggregated data collected on March 25 and 26, 2023. The directions of pedestrians and vehicles, as shown in Figure 6, are determined by using the coordinate system in Figure 19.

Table 4 reveals a generally stable distribution. None of the proportions exceed 50% for any given time of the day, indicating a relatively balanced traffic pattern. However, a discernible trend emerges with increased pedestrian and vehicular volumes observed during the afternoon hours compared with the morning hours. Also, more regular pedestrians and jaywalkers came from the P1(J1) direction in the morning hours, while the traffic shifted toward the opposite direction in the

afternoon hours. This is explained by the presence of the parking building, as shown in Figure 6, which influences the flow of regular pedestrians and jaywalkers in the vicinity of the crosswalk.

Table 4. Variability of vehicular and pedestrian volumes at the RRFB-controlled intersection

Time of the day (TD)	Vehicle direction			Pedestrian direction			
	V1	V2	V3	P1	P2	J1	J2
07:00 a.m. - 09:00 a.m. (TD1)	381 (8.8%)	83 (25.5%)	395 (10.8%)	45 (14.1%)	36 (10.7%)	23 (12.9%)	16 (6.5%)
09:00 a.m. - 11:00 a.m. (TD2)	458 (10.6%)	79 (24.2%)	562 (15.4%)	68 (21.3%)	52 (15.4%)	35 (19.7%)	23 (9.3%)
11:00 a.m. - 01:00 p.m. (TD3)	1002 (23.2%)	71 (21.8%)	801 (21.9%)	60 (18.8%)	57 (16.9%)	27 (15.2%)	45 (18.1%)
01:00 p.m. - 03:00 p.m. (TD4)	736 (17.1%)	53 (16.3%)	690 (18.9%)	57 (17.9%)	74 (21.9%)	26 (14.6%)	63 (25.4%)
03:00 p.m. - 05:00 p.m. (TD5)	805 (18.7%)	23 (7.1%)	590 (16.1%)	42 (13.2%)	61 (18.0%)	42 (23.6%)	53 (21.4%)
05:00 p.m. - 07:00 p.m. (TD6)	832 (19.3%)	17 (5.2%)	618 (16.9%)	47 (14.7%)	58 (17.2%)	25 (14.0%)	48 (19.4%)
Total per direction (TD1-TD6)	4314	326	3656	319	338	178	248
Total (all directions)	8296			657		426	

Note: V1, V2, and V3 are vehicle directions, and P1 (J1) and P2 (J2) are regular pedestrian/jaywalker crossing directions, as indicated in Figure 6. Values in parentheses represent the proportions of traffic volumes.

5.2.2. Vehicle and Pedestrian Trajectories at the RRFB-Controlled Intersection

Figure 20 and Figure 21 are snapshots of pedestrian and vehicle trajectories in the crosswalk zone at the Cabarrus Ave and Market St intersection. The middle bottom point of the bounding box serves as the reference point for locating pedestrians and vehicles on the video frames (Zhang et al., 2021b). Trajectories were extracted by tracking the movements of pedestrians and vehicles across consecutive frames over time. They show the paths pedestrians and vehicles followed as they navigated through the crosswalk zone.

Figure 20. Snapshot of pedestrian trajectories at the RRFB-controlled intersection

Figure 21. Snapshot of vehicle trajectories at the RRFB-controlled intersection

As can be seen in Figure 20, there were many jaywalkers. The proportion of jaywalkers is higher in the crosswalk zone of the Cabarrus Ave & Market St intersection when compared with the fixed-cycle intersection. This trend can be seen by comparing Table 4 with Table 1. It appears that pedestrians found it more convenient to jaywalk than reach the crosswalk and engage the RRFB.

5.2.3. Average Pedestrian and Vehicle Crossing Speeds at the RRFB-Controlled Intersection

5.2.3.1. Average pedestrian crossing speeds at the RRFB-controlled intersection

Similar to the findings observed at the fixed cycle intersection, the results of the two-way ANOVA revealed that average pedestrian crossing speeds are primarily influenced by the time of the day rather than the direction of crossing. The F-statistic for travel direction yielded a value of 0.02, indicating a lack of statistical significance, as supported by the corresponding p-value of 0.276. In contrast, the F-statistic for the time of day was 6.33, indicating a significant effect on pedestrian crossing speeds. This observation is reinforced by the p-value of 0.03, further substantiating the statistical significance of the relationship between the time of day and pedestrian crossing speeds.

The distribution of average pedestrian crossing speeds for different times of the day is illustrated in Figure 22. The analysis indicates no significant differences in the average pedestrian crossing speeds across the considered six times of the day. This implies that pedestrian walking speeds remain relatively consistent throughout the day without any notable variations observed.

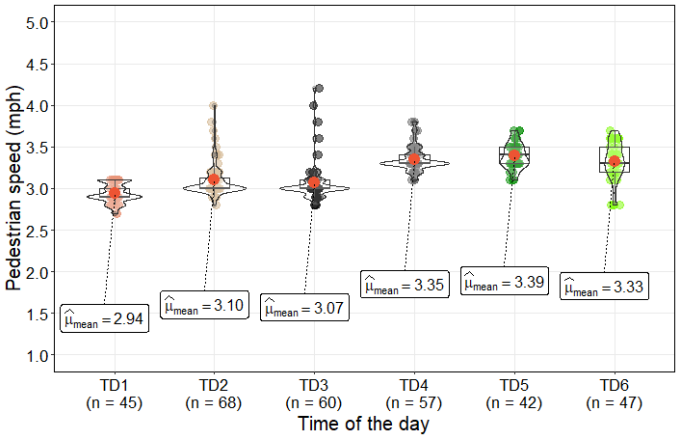

(a) P1 direction

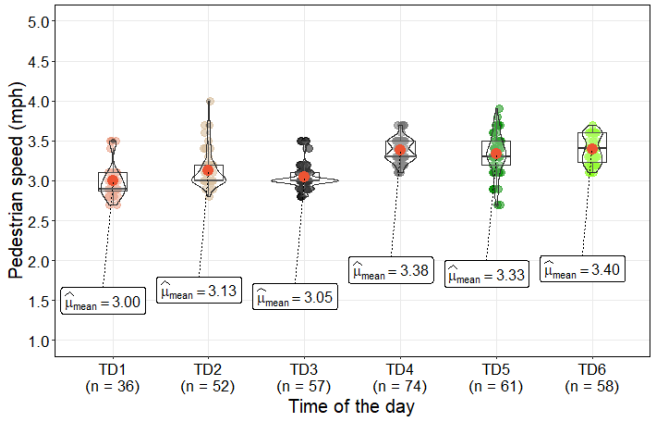

(b) P2 direction

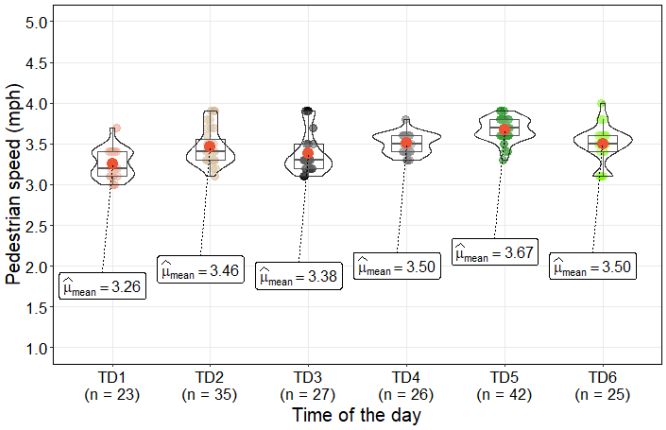

(c) J1 direction

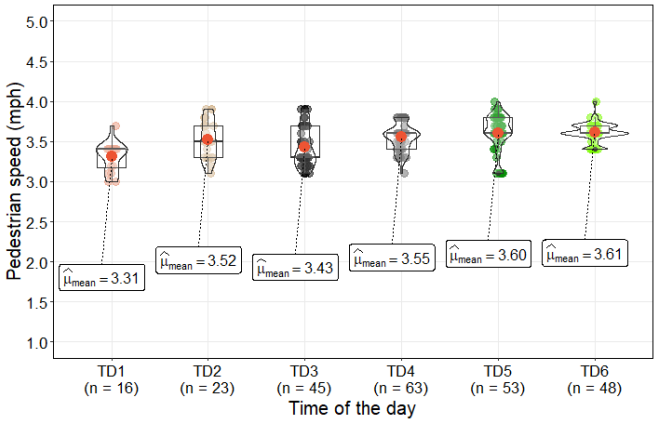

(d) J2 direction

Figure 22. Average pedestrian speeds at the RRFB-controlled intersection by time of the day and crossing direction

The results reveal that overall, the speed of jaywalkers is higher compared to those of regular pedestrians. This behavior can be attributed to their awareness of violating traffic rules by not using the designated crosswalk. Jaywalkers aim to minimize their exposure to potential conflicts with vehicles, leading them to adopt a quicker pace (Zhou et al., 2013). Additionally, the analysis of pedestrian speeds reveals that the highest recorded crossing speed for both regular pedestrians and jaywalkers is 4.2 mph.

5.2.3.2. Average vehicle speeds at the location with a RRFB

Figure 23 provides a visual representation of the average speeds observed for vehicles at the RRFB-controlled intersection throughout the day, grouped according to their specific travel directions. This figure offers valuable insights into the dynamic nature of speed variations over time at that specific intersection.

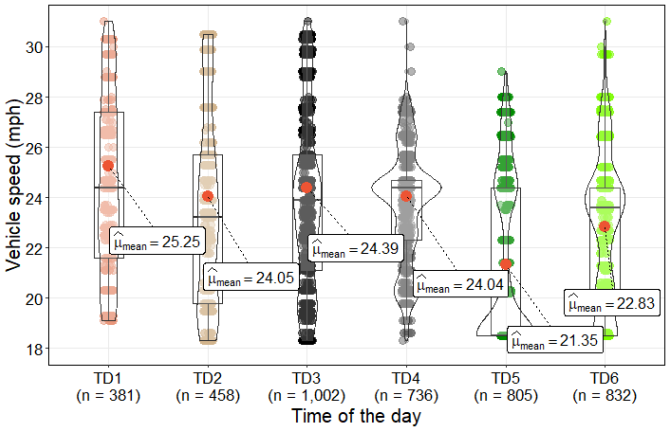

(a) V1 direction

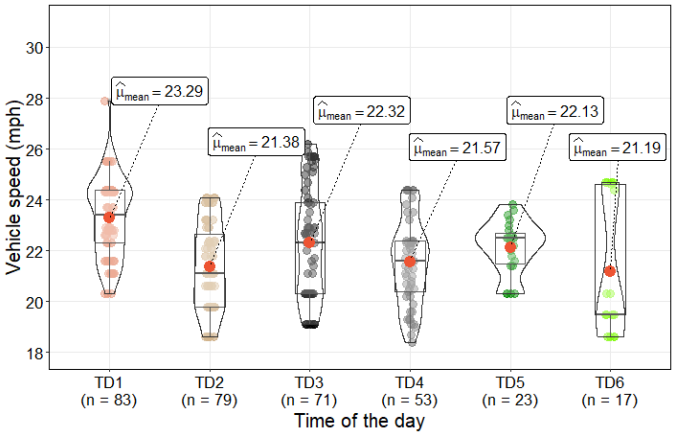

(b) V2 direction

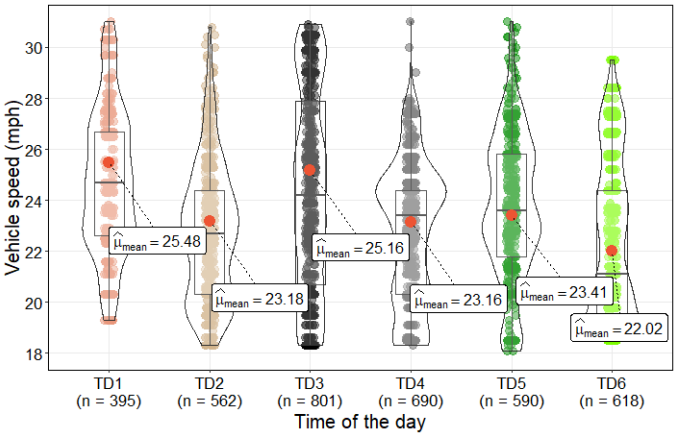

(c) V3 direction

Figure 23. Average vehicle speeds at the RRFB-controlled intersection by time of the day and crossing direction

The maximum average speed attained by vehicles in the eastbound and westbound directions of Cabarrus Ave (V1 and V3) was 37.8 mph. Figure 23(a) and Figure 23(c) show the distribution of the average vehicle speeds by time of the day. Additionally, the highest average speed recorded for vehicles traveling toward the public parking building (V3) was 27.9 mph, as illustrated in Figure 23(b).

Figure 23 provides insightful information indicating that the mean of all average speeds surpasses the designated 20-mph speed limit. The results from the two-way ANOVA indicate that travel direction and time of day significantly influence the average vehicle speeds. This is supported by the F-statistic values of 5275.8 for travel direction and 102.4 for time of the day, along with their corresponding p-values, which are statistically significant at the 99% confidence level.

A substantial proportion of drivers, specifically 6505 individuals, were found to exceed the designated 20-mph speed limit. This proportion accounted for approximately 78% of the total number of vehicles observed during the study period. The high percentage of drivers exceeding the speed limit at the RRFB-controlled intersection alerts a safety issue. It implies that many drivers did not adhere to the speed limit despite the RRFB system. This calls for further analysis and measures to address driver behavior and promote greater compliance with speed regulations in conjunction with the RRFB. Efforts such as increased enforcement, public awareness campaigns, and potential modifications to the traffic environment may be necessary to mitigate the risks associated with speeding at RRFB-controlled intersections.

5.2.4. Macroscopic and Microscopic Validation for the RRFB-Controlled Intersection

The calibration process involved incorporating the longitudinal and transversal dimensions of the crosswalk zone into the plane calibration in Kinovea software, as shown in Figure 24. A grid of 15x15, as shown in Figure 24, was found suitable for the task. This grid facilitated accurate mapping and alignment of the video footage, allowing for precise manual tracking and analysis.

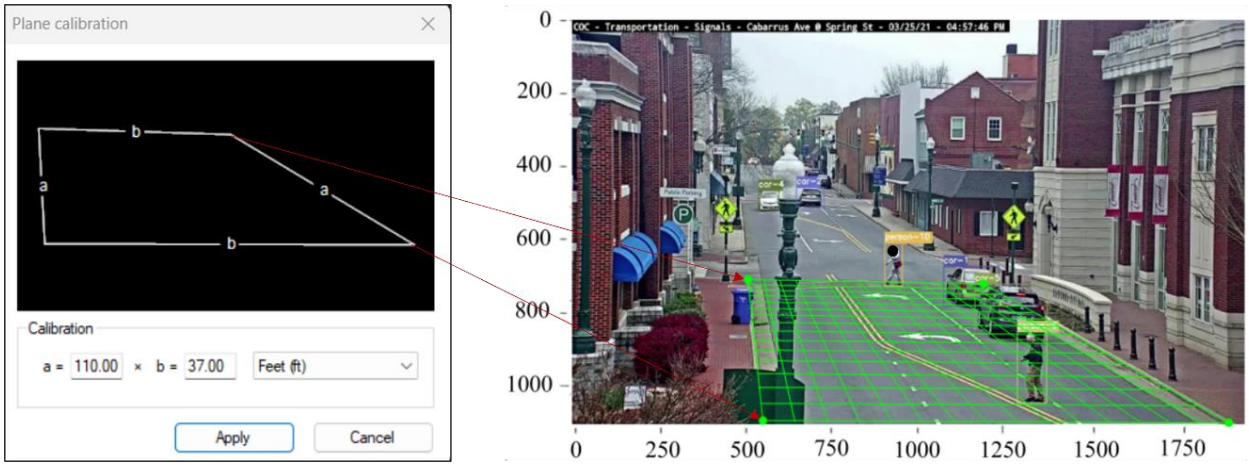

Figure 24. Grid overlaid over a video frame of the RRFB-controlled intersection

Each point on the grid underwent a conversion process to translate its pixel-based coordinates into real-world coordinates. Subsequently, manual tracking of pedestrians and vehicles was performed frame by frame. The number of frames analyzed in the Kinovea software aligned with those used in the automated tracking-by-detection approach, focusing on video sections chosen for validation purposes. This systematic tracking process ensured consistency and reliability in the data analysis.

5.2.4.1. Pedestrian-vehicle conflicts at the RRFB-controlled intersection

The speeds obtained through tracking-by-detection were compared with the manually extracted speeds. Figure 25 and Figure 26 show the relationship between the automatically extracted speeds and the manually measured speeds of pedestrians and vehicles.

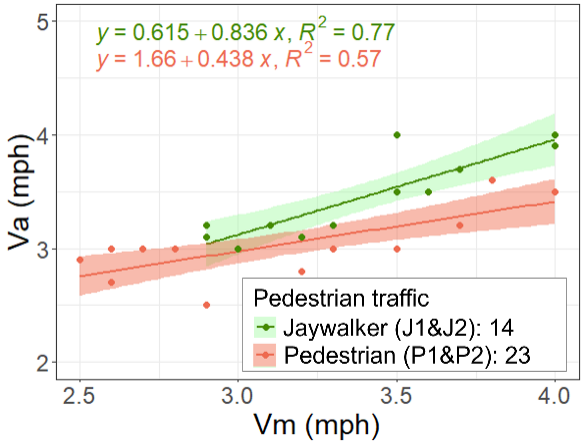

Figure 25. Pedestrian speed validation for the RRFB-controlled intersection

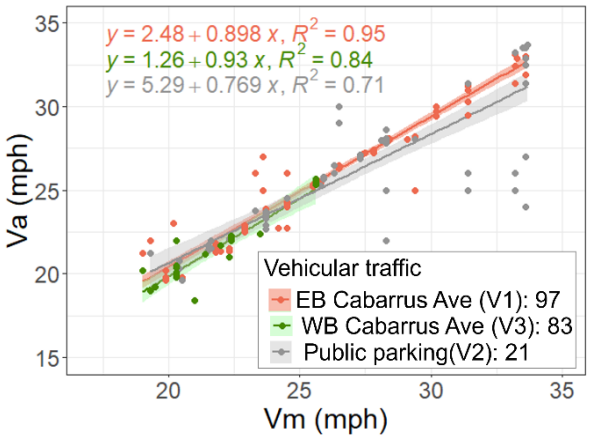

Figure 26. Vehicle speed validation for the RRFB-controlled intersection

To assess the accuracy of average vehicle and pedestrian speeds, the validation was conducted using the maximum count of vehicles and pedestrians within a 15-minute interval. This interval is commonly used to evaluate traffic dynamics and patterns. For average pedestrian crossing speeds, the analysis considered the maximum count of pedestrians and jaywalkers crossing the road, irrespective of their crossing direction.

The validation metrics are presented in Table 5. These metrics, such as MRE, RPE, and RAE, offer valuable insights into the accuracy and reliability of predicted speeds. The results

indicate that the computed average speeds for both vehicles and pedestrians exhibit an acceptable level of performance metrics, providing confidence in the accuracy of the obtained speed estimates.

Table 5. Validation metrics of average speeds for the RRFB-controlled intersection

Metric	Vehicles			Regular pedestrians	Jaywalkers
	Eastbound Cabarrus Ave	Public parking building	Westbound Cabarrus Ave		
R-square (%)	95.1	71.2	84.4	57.3	76.8
MRE (%)	4.2	10.1	6.3	12.3	6.6
RPE (%)	5.4	9.6	7.3	9.4	6.1
RAE (%)	4.3	11.6	4.9	10.8	5.6

5.2.4.2. Accuracy of Pedestrian and Vehicle Trajectories

The longitudinal and transversal trajectories of vehicles and pedestrians were subjected to the Shapiro-Wilk normality test. The purpose of this test was to determine if the distribution of points in these trajectories significantly deviated from a normal distribution. The findings presented in Table 6 reveal that the p-values associated with the test were greater than 0.05. This indicates no significant deviation from normality in the distribution of points for both vehicle and pedestrian trajectories. Consequently, the distribution of the data can be considered a normal distribution.

A paired sample t-test was conducted to analyze and compare the two sets of paired samples: the automatically extracted longitudinal and transversal points versus the manually extracted longitudinal and transversal points. This test was to determine if there was a statistically significant difference between the two sets of data. The findings, as presented in Table 6, reveal that the p-values associated with the t-test were greater than 0.05. This indicates that there was no

significant difference between the paired samples. In other words, the automated and manual extraction of longitudinal and transversal points yielded similar results.

Table 6. Results about microscopic validation for the RRFB-controlled intersection

Road user direction	Longitudinal trajectory		Transversal trajectory	
	Shapiro-Wilk normality test	Paired sample t-test	Shapiro-Wilk normality test	Paired sample t-test
Vehicle direction				
V2	0.54	0.07	0.54	0.32
V1	0.92	0.54	0.64	0.43
V3	0.13	0.09	0.21	0.07
Pedestrian direction				
P1 and P2	0.07	0.24	0.32	0.36
J1 and J2	0.23	0.87	0.54	0.08

5.2.5. Pedestrian-Vehicle Conflicts at the RRFB-Controlled Intersection

This subsection is dedicated to evaluating pedestrian-vehicle conflicts at the RRFB-controlled intersection. The evaluation was conducted using PETs, and the pedestrian-vehicle conflicts were analyzed.

The distribution of PETs is depicted in Figure 27, reflecting the severity levels of pedestrian-vehicle conflicts observed at the RRBF-controlled intersection. Out of the 1,083 pedestrians observed during the study, 511 pedestrians were involved in conflicts with vehicles while crossing the road, as indicated by PET values of less than 6 seconds. This subset accounted for approximately 47.2% of conflicts involving all pedestrians who crossed the road. Within these traffic conflicts, 218 instances involved jaywalkers, constituting about 42.7% of the total observed conflicts. An interesting observation is that despite the presence of the RRFB, the Cabarrus Ave & Market St intersection experienced more conflicts between regular pedestrians and vehicles than the fixed-cycle intersection. This finding highlights the need for further examination and potential

improvements to mitigate conflicts and enhance pedestrian safety at the RRFB-controlled intersection.

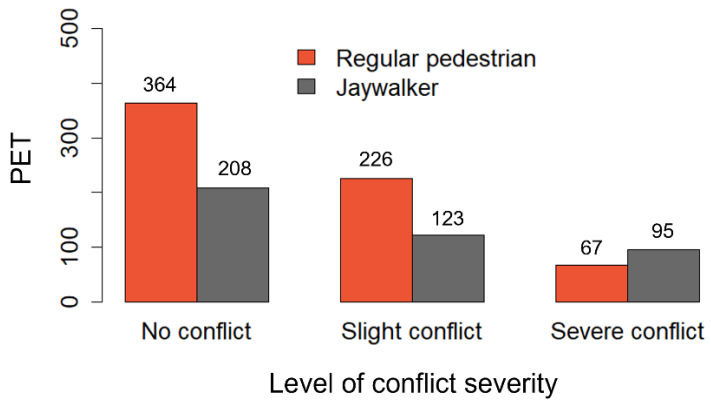

Figure 27. Distribution of PETs for the RRFB-controlled intersection by type of pedestrian and level of conflict severity

Out of the observed 657 regular pedestrians, 391 pedestrians were males, representing approximately 59.5% of the regular pedestrian population. Similarly, among the observed 426 jaywalkers at the same intersection, 231 were males, accounting for about 54.2% of the jaywalking incidents. These observations highlight a gender imbalance in pedestrian behavior, with males being more prevalent in regular pedestrian crossings and jaywalking. Understanding these gender-specific patterns can provide valuable insights into potential factors influencing pedestrian behavior and safety, thus facilitating targeted interventions and initiatives to address any associated risks of pedestrian-vehicle conflicts.

Another observation is related to the vehicle speeds. Approximately 78% of drivers exceeded the 20-mph speed limit. As jaywalking is frequent at the RRFB-controlled intersection, there is a serious threat to pedestrian safety. Ensuring compliance with the speed limit is crucial for safeguarding pedestrian safety and mitigating the risks associated with jaywalking incidents.

CHAPTER 6: PREDICTING PEDESTRIAN-VEHICLE CONFLICTS

This chapter focuses on the prediction of the severity of pedestrian-vehicle conflicts using LSTM neural network models. Variables, including pedestrian, vehicle, and signal timing-related factors, identified as relevant through the extensive review of existing literature discussed in Chapter 2, were considered to develop these models.

These predictions are based on pedestrian and vehicle trajectories. These trajectories should be extracted μ seconds before they reach the conflicting zones. This research used the value of 2s since it corresponds to the driver reaction time (Obeid et al., 2017; Wilson et al., 1997). In a CAV environment, these LSTM neural network models will warn the driver 2s ahead about a potential conflict with a pedestrian.

6.1. Predicting Pedestrian-Vehicle Conflicts at the Fixed-Cycle Intersection

The developed LSTM neural network models predict either of the three levels of pedestrian-vehicle conflicts: no conflict, slight conflict, and severe conflicts. Pedestrian gender, pedestrian speed, pedestrian crossing direction, pedestrian speed, whether the pedestrian jaywalks or not, pedestrian red-light violations, the x and y coordinates of pedestrians and vehicles, vehicle speed, and vehicle direction were used as predictors of the level of severity of pedestrian-vehicle conflicts.

Unlike other variables, pedestrian gender was manually extracted from the video data. Also, pedestrian speed and the x and y coordinates of pedestrians and vehicles were scaled. Scaling the variables helps ensure that all the features contribute equally to the model's learning process,

preventing those with larger magnitudes from dominating the training process. Vehicle speed is treated as a binary outcome, specifically categorized as greater or less than the 25-mph speed limit.

Table 7 summarizes all the variables used in the LSTM neural network model for the fixed-cycle intersection.

Table 7. Data summary for pedestrian-vehicle conflict severity prediction at the fixed-cycle intersection

Variable	Distribution
PET	No conflict (PET: >6s) = 494, slight conflict (>3s & ≤6s) =167, and severe conflict (≤3s) =83
Scaled pedestrian speed (mph)	(min=0, max=1)
Scaled X coordinate of pedestrian location	(min=0, max=1)
Scaled Y coordinate of pedestrian location	(min=0, max=1)
Pedestrian gender	Male = 440 and Female = 304
Pedestrian crossing direction	P1 or J1 = 398 and P2 or J2 = 346
Jaywalking	Yes = 136 and No = 608
Pedestrian red-light violation	Yes = 231 and No = 513
Scaled X coordinate of vehicle location	(min=0, max=1)
Scaled Y coordinate of vehicle location	(min=0, max=1)
Vehicle speed (mph)	"≤25 mph"=274 and ">25 mph"=470
Vehicle direction	V1=339, V2=309, and V3=96
Time of the day	TD1=71, TD2=80, TD3=122, TD4=160, TD5=159, and TD6=152

6.1.1. LSTM Neural Network Model Training for the Fixed-Cycle Intersection

After slicing and stacking the features from different time slices, the dataset used in this research included 78,120 records. This process of slicing and stacking involves organizing the sequential input data in a manner suitable for training an LSTM neural network model, known for its ability to effectively capture dependencies and patterns in sequential data.

The dataset is labeled with three targeted classes, namely no conflict, slight conflict, and severe conflict. These classes exhibit a ratio of approximately 32:3:1, respectively, indicating a significant majority of records labeled as no conflict. This distribution reflects the varying levels of conflict severity encountered in the dataset. By employing the technique of slicing and stacking the data, the sequential nature of the input is preserved, enabling the LSTM neural network model to capture temporal dependencies and patterns.

Eighty percent of the dataset was used as the training dataset. An over-sampling technique, Synthetic Minority Over-Sampling Technique (SMOTE), was applied to the training data to address the class imbalance issue. SMOTE, introduced by Chawla et al. (2002), is a popular method used to augment the number of records belonging to the minority classes, slight conflict, and severe conflict in this research. This synthetic data creation process is designed to ensure that the distribution of the three classes in the training data becomes balanced, with a ratio of 1:1:1. In other words, the number of records in each of the three classes, no conflict, slight conflict, and severe conflict, are equalized.

The selected hyperparameters and their corresponding values for the LSTM neural network model are presented in Table 8. These hyperparameters were chosen after thoroughly comparing the model's performance across different values within the tuning range. The LSTM neural network model reached an AUC value of 81.7% on the training dataset.

A batch size value of 1500 was determined to be the most suitable. This indicates that 1500 records are processed together in each iteration during training. The number of LSTM neural network units, which determines the complexity and capacity of the LSTM neural network layers, was set to 128. This value was found to yield optimal performance for the model. The learning rate, an essential parameter that affects the speed and stability of the model's training, was set at

0.001. This value was chosen after evaluating the model's performance with various learning rates within the tuning range. The number of epochs, representing the number of times the model goes through the entire training dataset, was determined as 80. This value strikes a balance between ensuring sufficient training iterations and avoiding overfitting.

Table 8. LSTM neural network hyperparameter tuning for the fixed-cycle intersection

Parameter	Range	Selected value
Batch size	[100, 500, 1000, 1500, 5000]	1500
# of LSTM units	[32, 64, 128, 256, 1024]	128
Learning rate	[0.0005, 0.001, 0.005, 0.01]	0.001
# of epochs	[10, 20, 50, 100, 150, 200, 250]	80
Dropout rate	[0.1, 0.2, 0.3, 0.4, 0.5]	0.2
Optimizer	[SGD, Adagrad, Adam, SGD]	Adam
Activation	[Linear, Sigmoid, Relu, Tanh, Softmax]	Tanh

The dropout rate, a regularization technique to prevent overfitting, was set to 0.2. This value helps improve the model's generalization ability by randomly dropping out 20% of the connections between LSTM neural network layers. The optimizer selected for the model is Adam, known for its efficiency in optimizing deep learning models. The activation function chosen is Tanh, which introduces non-linearity into the model's computations.

The proposed LSTM neural network model architecture comprises three stacked LSTM layers, one dense layer, and two dropout layers. The input of the first layer of the LSTM neural network is in three dimensions, consisting of the batch size (1500), the number of time slices (3), and the number of independent variables (12). This input structure ensures that the model can process and analyze the sequential and multi-dimensional nature of the input data effectively.

The LSTM neural network model can efficiently capture the complexities and patterns in the data, leading to accurate predictions and reliable analysis of pedestrian-vehicle conflicts, by fine-tuning these hyperparameters and designing a suitable architecture.

6.1.2. LSTM Neural Network Model Evaluation for the Fixed-Cycle Intersection

Twenty percent of the 78,120 records were used for model evaluation without addressing the imbalance issue. The test dataset is representative of the original dataset, including the imbalanced distribution of the three classes: no conflict, slight conflict, and severe conflict. This means that the proportion of records for each class in the test dataset remains the same as in the original dataset.

The performance metrics are presented in Table 9. They are computed from Equations (8)-(11). In this research, the samples are distributed across three classes, so the average values of the metrics are calculated from each class and used for evaluation. Table 9 presents individual performance metrics and the overall performance metrics of the proposed LSTM neural network model.

Table 9. LSTM neural network model performance metrics for the fixed-cycle intersection

Training (%)		Testing (%)				
		Conflict level	No conflict	Slight conflict	Severe conflict	All
AUC	81.7	Accuracy	-	-	-	86.5
		Recall	86.4	74.7	68.9	76.7
		Precision	83.4	83.1	75.3	80.6
		F1-score	84.9	78.7	72	78.5

Due to the imbalanced distribution of the data, with most instances belonging to the no conflict class, achieving high precision and recall for the severe conflict class presents a challenge.

Compared to the other levels of conflict severity, the performance metrics for severe conflicts are relatively lower, though still within an acceptable range.

Since the cost of a severe conflict is high (higher likelihood of being a crash), the model was developed while ensuring that as many positive instances as possible are correctly identified (higher recall) without compromising the trade-off between recall and precision. The highest value that could be obtained on the dataset was a recall of 68.9% on severe conflicts, which is considered acceptable. The LSTM neural network model achieved a recall of 76.7% over both classes. Moreover, the precision value is 80.6% and the F1 score is 78.5%. The model achieved an overall accuracy of 86.5% on the test data set.

6.2. Predicting Pedestrian-Vehicle Conflicts at the RRFB-Controlled Intersection

An LSTM neural network model was also developed to predict the severity of pedestrian-vehicle conflicts at the RRFB-controlled intersection. Pedestrian gender, pedestrian crossing direction, pedestrian speed, whether the pedestrian jaywalks or not, the x and y coordinates of pedestrians and vehicles, vehicle location, vehicle speed, vehicle direction, and time of the day were used as variables.

Unlike other variables, pedestrian gender was manually extracted from the video data. Also, pedestrian speed, the x and y coordinates of pedestrians and vehicles were scaled. Vehicle speed was treated as a binary outcome, specifically categorized as greater or less than the 20-mph speed limit.

Table 10 summarizes all the variables in the LSTM neural network model developed for the RRFB-controlled intersection.

Table 10. Data summary for pedestrian-vehicle conflict severity prediction at the RRFB-controlled intersection

Variable	Distribution
PET	No conflict (PET: >6s) = 572, slight conflict (>3s & ≤6s) =349, and severe conflict (≤3s) =162
Scaled pedestrian speed (mph)	(min=0, max=1)
Scaled X coordinate of pedestrian location	(min=0, max=1)
Scaled Y coordinate of pedestrian location	(min=0, max=1)
Pedestrian gender	Male = 622 and Female = 461
Pedestrian crossing direction	P1 or J1 = 497 and P2 or J2 = 586
Jaywalking	Yes = 426 and No = 657
Scaled X coordinate of vehicle location	(min=0, max=1)
Scaled Y coordinate of vehicle location	(min=0, max=1)
Vehicle speed (mph)	"≤20 mph" = 436 and ">20 mph" = 647
Vehicle direction	V1=486, V2=62, and V3=535
Time of the day	TD1=141, TD2=217, TD3=173, TD4=195, TD5=292, and TD6=65

6.2.1. LSTM Neural Network Model Training for the RRFB-Controlled Intersection

There are 113,715 records in the dataset after the slicing and stacking process. The dataset is distributed across the target variable, i.e., pedestrian-vehicle conflict severity, with a ratio of approximately 11:2:1 for no conflicts, slight conflicts, and severe conflicts, respectively. This distribution reflects the varying levels of conflict severity encountered in the dataset.

Eighty percent of the dataset was used for training the LSTM neural network model. SMOTE was used to address the imbalance issue toward the no conflict class, such as the ratio across the three categories being equalized.

The hyperparameters for the selected LSTM neural network model are provided in Table 11. These hyperparameters were selected after comparing the model's performance for different values within the tuning range. The LSTM neural network model reached an AUC value of 78.5% on the training dataset.

Table 11. LSTM neural network hyperparameter tuning for the RRFB-controlled intersection

Parameter	Range	Selected value
Batch size	[100, 500, 1000, 1500, 5000]	1000
# of LSTM units	[32, 64, 128, 256, 1024]	256
Learning rate	[0.0005, 0.001, 0.005, 0.01]	0.005
# of epochs	[10, 20, 50, 100, 150, 200, 250]	120
Dropout rate	[0.1, 0.2, 0.3, 0.4, 0.5]	0.4
Optimizer	[SGD, Adagrad, Adam, SGD]	Adam
Activation	[Linear, Sigmoid, Relu, Tanh, Softmax]	Tanh

A batch size of 1000, 256 LSTM neural network units, a learning rate of 0.005, 120 epochs, and a dropout rate of 0.4 yielded the best performance for the model. The Adam optimizer and Tanh activation functions were identified as the most suitable choices for the model.

The proposed LSTM neural network model architecture comprises three stacked LSTM layers, one dense layer, and two dropout layers. This architecture allows the model to effectively capture sequential dependencies and patterns within the data, leading to accurate predictions.

The input of the first layer of the LSTM neural network is in three dimensions, consisting of the batch size (1000), the number of time slices (3), and the number of independent variables (11). This input structure enables the model to process the sequential and multi-dimensional nature of the data effectively.

6.2.2. LSTM Neural Network Model Evaluation for the RRFB-Controlled Intersection

Twenty percent of the 113,715 records were used for model evaluation without addressing the imbalance issue. The performance metrics of the developed model are presented in Table 12. The average values of the metrics calculated from each class were used for evaluation. These

averages represent the overall performance metrics of the proposed LSTM neural network model for the RRFB-controlled intersection.

Table 12. LSTM neural network model performance metrics for the RRFB-controlled intersection

Training (%)		Testing (%)				
		Conflict level	No conflict	Slight conflict	Severe conflict	All
AUC	78.5	Accuracy	-	-	-	73.8
		Recall	71.9	74.8	66.5	71.1
		Precision	72.9	68.3	76.4	72.5
		F1-score	72.4	71.6	78.0	74.0

As severe conflicts could lead to crashes, reaching an acceptable recall value was of high importance. The proposed LSTM neural network model for the RRFB-controlled intersection reached a recall of 66.5% on severe conflicts.

Given the likelihood of the severity of conflicts that could lead to crashes, achieving an acceptable recall value was of utmost importance. In the proposed LSTM neural network model for the RRFB-controlled intersection, the performance evaluation on severe conflicts yielded a recall value of 66.5%. This recall value indicates the model's ability to correctly identify a substantial proportion of severe conflict instances out of the total occurrences. The model demonstrates a reasonable capacity to detect and classify instances with a higher risk of potential crashes by achieving a recall of 66.5% on severe conflicts. The model achieved a recall of 71.1% over the three conflict severity levels with a precision and a F1 score of 72.5% and 74.0%, respectively. The overall accuracy on the test dataset is 73.8%.

CHAPTER 7: EFFECTS ON PEDESTRIAN-VEHICLE CONFLICTS

This chapter focuses on modeling the effects of pedestrian, vehicle, and signal timing-related factors on the severity of pedestrian-vehicle conflicts at the fixed-cycle intersection and the RRFB-controlled intersection. The adjacent-category approach was used for this purpose. Specifically, AC, PAC, and ACPPC were developed. These three models are explained in Chapter 3. Compared to the AC model, the PO assumption is relaxed in the case of the PAC and the ACPPC models. However, in the PAC model, the PO assumption is relaxed only for some variables, while all the independent variables in the ACPPC model vary freely, with some variables varying by a common factor. This means that the relationship between the independent variables and the odds of a pedestrian-vehicle conflict occurring at a particular level of conflict severity is not constant across all levels of severity of pedestrian-vehicle conflicts.

In the proposed adjacent-category approach, two scenarios were of interest as there are three levels of severity of pedestrian-vehicle conflicts. In the first scenario (scenario 1), the magnitude and the direction of the effects of pedestrian, vehicle, and signal timing-related factors were measured based on the no conflict level.

7.1. Effects on Pedestrian-Vehicle Conflicts at the Fixed-Cycle Intersection

Eleven variables pertaining to pedestrian, vehicle, and signal timing-related factors were used in the AC, PAC, and ACPPC models. These variables include time of the day, vehicle direction, vehicle speed, pedestrian gender, pedestrian speed, pedestrian crossing direction, jaywalking, pedestrian red-light violation, green time, yellow time, and red time.

The effect of time of the day on the severity of pedestrian-vehicle conflicts was measured by comparing it to the reference time of the day (from 7:00 a.m. to 9:00 a.m., also referred to as TD1 in this research). Similarly, the effect of the vehicle direction was measured using the southbound Union St (V1) as the reference direction. Vehicle speed was used as a binary variable in the models, distinguishing between speeds below or equal to 25 mph and speeds exceeding 25 mph. The models also examined the effects of pedestrian gender by using males as the reference category. Pedestrian speeds ranged from 2.3 to 4.5 mph. The effect of the pedestrian crossing direction was measured by comparing it to the reference direction P1 or J1, as shown in Figure 5. Jaywalking was also treated as a binary variable in the models.

Signal timing-related factors such as green time, yellow time, and red time were modeled as countdown timers to understand the impact of the time remaining of a particular signal timing on the severity of pedestrian-vehicle conflicts. For example, a yellow time of 4 s means the signal state is currently yellow and has 4s remaining.

The traffic cycle has a total duration of 60 seconds at the fixed-cycle signalized intersection under investigation. This cycle includes distinct phases for vehicles, comprising a 35-second green phase, a 5-second yellow phase, and a 20-second red phase. These time allocations indicate how long each phase lasts and provide important context for analyzing the effects of signal timing-related factors on pedestrian-vehicle conflicts.

7.1.1. Model Results for the Fixed-Cycle Intersection

This subsection presents the results of the AC, PAC, and ACPPC models developed for the fixed-cycle intersection. The Brant-Wald test was used to check the PO assumption. This test compared each of the three models with the unconstrained adjacent category model, i.e., a relaxing

of the PO model that allows for different coefficients at each level of the ordinal outcome variable. In other words, coefficients in the unconstrained adjacent category model (Model 4) were allowed to vary freely across scenarios 1 and 2.

In the AC model (Model 1), the PO assumption was applied for all eleven independent variables. Thus, only the intercept varied across scenarios 1 and 2. However, the Brant-Wald test showed that none of the p-values of the independent variables exceeded 0.05, implying the failure of the PO assumption. Consequently, the PAC and the APPC models (Model 2 and Model 3, respectively) were developed as alternatives.

In the PAC model, the PO assumption for vehicle speed, jaywalking, pedestrian red-light violation, green time, yellow time, and red time was relaxed and applied for time of the day, vehicle direction, pedestrian speed, pedestrian gender, and pedestrian crossing direction. In the ACPCC model, the PO assumption for each independent variable was relaxed. In other words, the effects of time of the day, vehicle direction, vehicle speed, pedestrian gender, pedestrian speed, and pedestrian crossing direction varied freely across scenarios, and the effects of jaywalking, pedestrian red-light violation, green time, yellow time, and red time varied by a common factor across the two scenarios. Jaywalking, pedestrian red-light violation, green time, yellow time, and red time varied by a common factor because the five variables are generally associated. For example, jaywalkers disregard traffic lights. The results of the four models are presented in Table 13.

Table 13. Results of adjacent-category models for the fixed-cycle intersection

		(1 = No conflict, 2 = Slight conflict, 3 = Severe conflict)							
		Model 1		Model 2		Model 3		Model 4	
		Adjacent category		Partial adjacent category		Adjacent category with partial proportionality constraints		Unconstrained adjacent category	
Variable		1 vs. 2 (Scenario 1)	2 vs. 3 (Scenario 2)	1 vs. 2 (Scenario 1)	2 vs. 3 (Scenario 2)	1 vs. 2 (Scenario 1)	2 vs. 3 (Scenario 2)	1 vs. 2 (Scenario 1)	2 vs. 3 (Scenario 2)
Time of the day									
	TD2	-0.002 (0.998)	-0.002 (0.998)	-0.002 (0.998)	-0.002 (0.998)	-0.018 (0.982)	0.027 (1.027)	-0.021 (0.979)	0.033 (1.034)
	TD3	-0.005 (0.995)	-0.005 (0.995)	0.003 (1.003)	0.003 (1.003)	0.006 (1.006)	0.016 (1.016)	0.009 (1.009)	0.017 (1.017)
	TD4	0.011 (1.011)	0.011 (1.011)	0.007 (1.007)	0.007 (1.007)	0.012 (1.012)	-0.005 (0.995)	0.015 (1.015)	-0.004 (0.996)
	TD5	-0.019 (0.981)	-0.019 (0.981)	-0.002 (0.998)	-0.002 (0.998)	-0.015 (0.985)	-0.001 (0.999)	-0.024 (0.976)	-0.007 (0.993)
	TD6	0.001 (1.001)	0.001 (1.001)	-0.003 (0.997)	-0.003 (0.997)	0.021 (1.021)	0.004 (1.004)	0.022 (1.022)	0.003 (1.003)
Vehicle direction									
	V2	-0.131 (0.877)	-0.131 (0.877)	-0.113 (0.893)	-0.113 (0.893)	-0.184 (0.832)	0.125 (1.133)	-0.192 (0.825)	0.136 (1.146)
	V3	-0.144 (0.866)	-0.144 (0.866)	-0.158 (0.854)	-0.158 (0.854)	0.163 (1.177)	0.128 (1.137)	0.177 (1.194)	-0.156 (0.856)
Vehicle speed (mph)		0.143 (1.154)	0.143 (1.154)	0.212 (1.236)	0.191 (1.210)	0.221 (1.247)	0.123 (1.131)	0.130 (1.139)	0.145 (1.156)
Pedestrian gender		0.348 (1.416)	0.348 (1.416)	0.359 (1.432)	0.359 (1.432)	0.407 (1.502)	0.428 (1.534)	0.311 (1.365)	0.437 (1.548)
Pedestrian speed (mph)		0.012 (1.012)	0.012 (1.012)	0.015 (1.015)	0.015 (1.015)	0.019 (1.019)	0.021 (1.021)	0.017 (1.017)	0.018 (1.018)
Pedestrian crossing direction		0.101 (1.106)	0.101 (1.106)	0.125 (1.133)	0.125 (1.133)	0.149 (1.161)	0.131 (1.140)	0.132 (1.141)	0.158 (1.171)
Jaywalking		0.098 (1.103)	0.098 (1.103)	0.096 (1.101)	0.092 (1.096)	0.095 (1.100)	0.091 (1.095)	0.093 (1.097)	0.098 (1.103)
Red-light violation		0.055 (1.057)	0.055 (1.057)	0.053 (1.054)	0.049 (1.050)	0.057 (1.059)	0.052 (1.053)	0.054 (1.055)	0.056 (1.058)
Green time remaining (s)		-0.039 (0.962)	-0.039 (0.962)	-0.042 (0.959)	-0.036 (0.965)	-0.034 (0.967)	-0.038 (0.963)	-0.046 (0.955)	-0.035 (0.966)
Yellow time remaining (s)		-0.221 (0.802)	-0.221 (0.802)	-0.174 (0.840)	-0.203 (0.816)	-0.189 (0.828)	-0.235 (0.791)	-0.174 (0.840)	-0.196 (0.822)
Red time remaining (s)		0.145 (1.156)	0.145 (1.156)	0.173 (1.189)	0.188 (1.207)	0.165 (1.179)	0.184 (1.202)	0.143 (1.154)	0.175 (1.191)
Constant		-2.368	-3.213	-2.634	-3.472	-2.964	-3.654	-3.053	-3.448
AIC		6318.235		6210.937		6148.703		6151.213	
BIC		6374.847		6301.046		6283.312		6296.659	

Note: N= 744; Values in parentheses are odds ratios; Bold values refer to significant variables (p-value <0.05 or less).

7.1.2. Discussion on the Model Results for the Fixed-Cycle Intersection

The results of all the adjacent category models presented in Table 13 are discussed in this subsection. Pedestrian-vehicle conflicts were modeled as an ordinal variable based on the PET values. The following were considered: no conflict (PET: >6s), slight conflict (>3s & ≤6s), and severe conflict (≤3s). Table 13 shows the magnitudes and the directions of the effects of various variables pertaining to pedestrian, vehicle, and signal timing-related factors.

The APPC model performed better than the other models, with the lowest Akaike information criterion (AIC) and Bayesian Information Criterion (BIC) values. Therefore, the discussion will be mainly based on the results from the ACPPC model (Model 3). Model 4 performed better than Model 2 and Model 1. Model 1 exhibited the highest AIC and BIC values, indicating that relaxing the PO assumption led to better-fitted models.

In summary, the positive signs of the coefficients in Table 13 increase the likelihood of higher PET levels (increase the likelihood of severe pedestrian-vehicle conflicts) while negative signs increase the likelihood of less severe pedestrian-vehicle conflicts.

Pedestrian-related factors vs. PETs. Model 3 revealed that pedestrian red-light violation does not significantly affect severe conflicts compared with slight conflicts. However, it increases the likelihood of a slight conflict by 5.9% when compared with a non-conflict situation. The non-significance of the effect on the severe conflict compared with the slight conflict situation and the relatively low percentage of the likelihood of a slight conflict in comparison to the non-conflict situation can be explained by the fact that pedestrians, including jaywalkers, more often try to be cautious by avoiding taking high-risk crossing. Past research found that pedestrian red-light violations are the primary cause for the higher occurrence of conflicts with vehicles at signalized intersections (Hussein et al., 2015).

Model 3 also revealed that jaywalkers are more at risk than pedestrians who violate the red light. This could be explained by the fact that drivers do not expect crossing pedestrians outside the crosswalk, especially when they have the ROW (green time for vehicles). Therefore, any conflict is more likely to be severe. The results show that jaywalking on a signalized intersection is more likely to increase the severe conflict situation by 9.5% compared to the slight conflict situation.

Vehicle-related factors vs. PETs. Vehicle speed increases the likelihood of slight conflicts and severe conflicts, compared with the adjacent lower severity level. In fact, a speed greater than 25 mph increases the likelihood of a slight conflict by about 24.7% compared with a non-conflict situation. On the other hand, the likelihood of a severe conflict increases by 13.1% compared with a slight conflict situation if a driver drives at a speed greater than 25 mph. Complying with the speed limit will help reduce the occurrence and the severity of slight and severe conflicts at fixed-cycle intersections. Driving at a speed lower than or equal to 25 mph was found to lead to fewer and less severe pedestrian-vehicle conflicts compared with higher vehicle speeds, as was observed by Zhang et al. (2015).

Signal timing-related factors vs. PETs. Table 13 shows that yellow time is negatively related to the severity of pedestrian-vehicle conflicts. The higher the yellow time, the higher the PET (the less severe the conflict). Increasing yellow time is less likely to lead to a riskier conflict. This is revealed by the odds ratio of the variable for the two scenarios of Model 3. In fact, increasing the yellow time by one second can improve the PET severity levels. Compared with a non-conflict situation, a one-second increase in yellow time can decrease the likelihood of a slight conflict by 17.2%. On the other hand, in comparison to a slight conflict situation, a one-second increase in yellow time can decrease the likelihood of a severe conflict situation by about 20.9%.

These findings align with previous research that reveals the benefit of extending the yellow time (Retting et al., 2008; Bonneson and Zimmerman, 2004).

Furthermore, increasing the yellow time can reduce the number of pedestrian red-light violations (Bonneson and Zimmerman, 2004). Hubbard et al. (2009) and Chen et al. (2014) found that some pedestrians arrive or start crossing late. Moreover, Chen et al. (2004) found that a larger yellow time may allow them to complete their crossing. However, according to the Manual on Uniform Traffic Control Devices (MUTCD) guidelines, the yellow time should not exceed 6s (MUTCD, 2009). This maximum yellow time was found adequate for warning drivers, allowing them to safely stop or clear the intersection before the conflicting traffic started moving.

In Model 3, the green time significantly affected slight conflicts than severe conflicts, compared with non-conflict and slight conflict situations, respectively. In fact, a one-second increase in the green time decreases the likelihood of a slight conflict. Compared with a non-conflict situation, a one-second increase in green time will drop the likelihood of a slight conflict by about 3.3%.

Overall, when comparing the magnitude of the effects of yellow and green times on the severity of pedestrian-vehicle conflicts, the results suggest an increase in the yellow time rather than the green time to decrease the likelihood of slight conflicts.

7.2. Effects on Pedestrian-Vehicle Conflicts at the RRFB-Controlled Intersection

To examine the effects of pedestrian, vehicle, and signal timing related factors, eight variables were used in the AC, PAC, and ACPPC models. These variables include time of the day, vehicle direction, vehicle speed, pedestrian gender, pedestrian speed, pedestrian crossing direction, jaywalking, and the flashing time.

The time of the day from 7:00 a.m. to 9:00 a.m. (TD1) was used as a reference to examine the effect of the time of the day on the severity of pedestrian-vehicle conflicts. Similarly, the vehicle lane toward the public parking building (V2) was used as a reference to examine the effect of the vehicle direction. Vehicle speed was treated as a binary variable with speeds below or greater than the 20-mph speed limit. Gender effects were examined, with males serving as the reference category. Pedestrian speeds ranged from 2.7 to 4.2 mph. The pedestrian direction P1 or J1, as shown in Figure 5, was used as a reference to measure the effect of pedestrian crossing direction on the severity of pedestrian-vehicle conflicts. Finally, the models also accounted for jaywalking as a binary variable.

The flashing time is modeled as a countdown timer to examine how the remaining time impacted the severity of pedestrian-vehicle conflicts. For example, once a pedestrian engages the RRFB at the Cabarrus Ave & Market St intersection, it flashes for 15s. During this period, vehicles approaching the intersection are expected to adhere to the traffic control device and remain in complete stop mode until the flashing time expires. This ensures that pedestrians have sufficient time to safely navigate the crosswalk and reach the other side of the road.

7.2.1. Model Results for the RRFB-Controlled Intersection

The AC, PAC, and ACPPC models were developed for the RRFB-controlled intersection. The Brant-Wald test was used to check the PO assumption. This test compared each of the three models with the unconstrained adjacent category model, i.e., a relaxing of the PO model that allows for different coefficients at each level of the ordinal outcome variable. In other words, coefficients in the unconstrained adjacent category model (Model 8) were allowed to vary freely across scenarios 1 and 2.

Three models were developed, including AC, PAC, and ACPPC models, to examine the effects of pedestrian, vehicle, and signal timing-related factors. The Brant-Wald test was used to assess the validity of the PO assumption. This test involved comparing three models with the unconstrained adjacent category model, referred to as Model 8. In Model 8, the PO assumption is relaxed, allowing for different coefficients to be estimated for each level of the ordinal outcome variable, i.e., the severity of pedestrian-vehicle conflicts.

In the AC model (Model 5), the PO assumption was held for all eight independent variables. In this model, the effects of these variables on the severity of pedestrian-vehicle conflicts are the same across different levels of conflict severity. However, the results of the Brant-Wald test revealed that none of the p-values associated with the independent variables exceeded the significance level of 0.05. Therefore, the PAC, and the APPC models, were developed.

In the PAC model (Model 6), the PO assumption was relaxed for some variables. Specifically, the PO assumption was not assumed for vehicle speed, jaywalking, and flashing time. Instead, the effects of these variables were allowed to vary freely across the two scenarios. On the other hand, the PO assumption was applied for time of the day, vehicle direction, pedestrian speed, pedestrian gender, and pedestrian crossing direction, assuming that the effects of these variables remain the same across the three levels of severity of pedestrian-vehicle conflicts.

In the ACPCC model (Model 7), the PO assumption for each independent variable was relaxed. In other words, the effects of time of the day, vehicle direction, vehicle speed, pedestrian gender, pedestrian speed, and pedestrian crossing direction varied freely, and the effects of jaywalking and flashing time vary by a common factor across the two scenarios. The variables jaywalking and flashing time vary by a common factor because the two variables are generally

associated as jaywalkers disregarded the presence of the RRFB. The results of the four models are presented in Table 14.

Table 14. Results of adjacent-category models for the RRFB-controlled intersection

		(1 = No conflict, 2 = Slight conflict, 3 = Severe conflict)							
		Model 1		Model 2		Model 3		Model 4	
		Adjacent category		Partial adjacent category		Adjacent category with partial proportionality constraints		Unconstrained adjacent category	
Variable		2 vs. 1 (Scenario 1)	3 vs. 2 (Scenario 2)	2 vs. 1 (Scenario 1)	3 vs. 2 (Scenario 2)	2 vs. 1 (Scenario 1)	3 vs. 2 (Scenario 2)	2 vs. 1 (Scenario 1)	3 vs. 2 (Scenario 2)
Time of the day									
	TD2	0.002 (1.002)	0.002 (1.002)	0.002 (1.002)	0.002 (1.002)	0.018 (1.018)	0.027 (1.027)	-0.021 (0.979)	0.033 (1.034)
	TD3	0.005 (1.005)	0.005 (1.005)	0.003 (1.003)	0.003 (1.003)	0.006 (1.006)	0.016 (1.016)	0.009 (1.009)	0.017 (1.017)
	TD4	-0.011 (0.989)	-0.011 (0.989)	-0.007 (0.993)	-0.007 (0.993)	-0.012 (0.988)	-0.005 (0.995)	-0.015 (0.985)	-0.004 (0.996)
	TD5	-0.019 (0.981)	-0.019 (0.981)	-0.002 (0.998)	-0.002 (0.998)	-0.015 (0.985)	-0.001 (0.999)	-0.024 (0.976)	-0.007 (0.993)
	TD6	-0.001 (0.999)	-0.001 (0.999)	-0.003 (0.997)	-0.003 (0.997)	-0.021 (0.979)	-0.004 (0.996)	-0.022 (0.978)	-0.003 (0.997)
Vehicle direction									
	V1	0.094 (1.099)	0.094 (1.099)	0.107 (1.113)	0.107 (1.113)	0.111 (1.117)	0.105 (1.111)	0.114 (1.121)	0.112 (1.119)
	V3	0.83 (2.293)	0.83 (2.293)	0.113 (1.120)	0.113 (1.120)	0.123 (1.131)	0.11 (1.116)	0.125 (1.133)	0.119 (1.126)
Vehicle speed (mph)		0.164 (1.178)	0.164 (1.178)	0.227 (1.255)	0.21 (1.234)	0.239 (1.270)	0.173 (1.189)	0.187 (1.206)	0.206 (1.229)
Pedestrian gender		0.323 (1.381	0.323 (1.381)	0.327 (1.387)	0.327 (1.387)	0.364 (1.439)	0.387 (1.473)	0.391 (1.478)	0.404 (1.498)
Pedestrian speed (mph)		0.016 (1.016)	0.016 (1.016)	0.019 (1.019)	0.019 (1.019)	0.021 (1.021)	0.018 (1.018)	0.018 (1.018)	0.017 (1.017)
Pedestrian crossing direction		0.093 (1.097)	0.093 (1.097)	0.098 (1.103)	0.098 (1.103)	0.116 (1.123)	0.995 (2.705)	0.119 (1.126)	0.108 (1.114)
Jaywalking		0.113 (1.120)	0.113 (1.120)	0.123 (1.131)	0.136 (1.146)	0.158 (1.171)	0.164 (1.178)	0.16 (1.174)	0.171 (1.186)
Flashing time remaining (s)		-0.123 (0.884)	-0.123 (0.884)	-0.192 (0.825)	-0.212 (0.809)	-0.231 (0.794)	-0.24 (0.787)	-0.212 (0.809)	-0.225 (0.799)
Constant		-2.125	-2.918	-2.486	-3.391	-2.775	-3.866	-2.943	-3.754
AIC		4219.39		4127.654		4099.238		3987.458	
BIC		4267.235		4256.168		4143.457		4085.346	

Note: N= 1083; Values in parentheses are odds ratios; Bold values refer to significant variables (p-value <0.05 or less).

7.2.2. Discussion on the Model Results for the RRFB-Controlled Intersection

This subsection is dedicated to discussing the results of the four adjacent category models developed for the RRFB-controlled intersection. The no conflict (PET: >6s), slight conflict (>3s & ≤6s), and severe conflict (≤3s) were considered as the three categories of the target variable. The magnitudes and the directions of the effects of the eight variables pertaining to pedestrian, vehicle, and signal timing-related factors are presented in Table 14.

The results indicate that the ACPPC model outperformed the other models, as evidenced by its lower AIC and BIC values. Therefore, the focus of the discussion will primarily revolve around the findings from the ACPPC model. The unconstrained model (Model 8) demonstrated better performance than the AC and the PAC models. The AC model exhibited the highest AIC and BIC values, suggesting that relaxing the PO assumption resulted in better-fitting models.

Overall, positive signs of the coefficients in Table 14 indicate an increase in the likelihood of higher levels of PET, corresponding to more severe conflicts. On the other hand, negative signs reveal an increase in the likelihood of less severe pedestrian-vehicle conflicts.

Pedestrian-related factors vs. PETs. The ACPPC model revealed that jaywalking significantly affects the safety of pedestrians at the RRBF-controlled intersection. Compared with a regular crossing situation, the likelihood of a slight conflict with a vehicle as compared with a non-conflict situation increases by 17.1% if a pedestrian decides to jaywalk. Moreover, the likelihood of a severe pedestrian-vehicle conflict involving a jaywalker increases by 17.8% compared with a slight conflict situation.

These results emphasize the importance of promoting safe crossing behaviors and discouraging jaywalking at the studied location. By raising awareness about the risks associated with jaywalking, measures can be taken to reduce the likelihood of conflicts.

Vehicle-related factors vs. PETs. The ACPPC model indicates that compared with V2, the vehicle directions V1 and V3 increase the likelihood of a slight conflict. These two directions adjacent to the sidewalk might explain why slight conflicts on these lanes are more likely to occur compared with the middle lane. In fact, the results indicate that slight conflicts are about 12.0% more likely to occur on the adjacent vehicle lanes compared with the non-conflict situation.

Also, driving above the speed limit increases the likelihood of both slight conflict and severe conflict. Driving at a speed higher than 20 mph increases the likelihood of a slight conflict by about 27.0% compared with a non-conflict situation. On the other hand, the likelihood of a severe conflict increases by 18.9% compared to the slight conflict situation. Therefore, it is important for drivers to comply with the speed limit as it lowers the severity of both slight and severe conflicts at the location with a RRFB.

Signal timing-related factors vs. PETs. Table 14 shows that the flashing time of the RRFB is negatively associated with the severity of pedestrian-vehicle conflicts. The higher the flashing time, the less severe the conflict. This is revealed by the odds values of the variable for the two scenarios. In fact, in comparison with the non-conflict (slight conflict) situation, the likelihood of a slight (severe) pedestrian-vehicle conflict decreases by 21.3% (19.3%) if the RRFB flashing time is increased by 1s.

These findings highlight the important role of the RRFB flashing time in enhancing pedestrian safety at the location. By increasing the duration of the flashing yellow phase, pedestrians are provided with more time to cross the road safely, reducing the probability of conflicts with vehicles reaching more severe levels.

CHAPTER 8: CONCLUSIONS

This research uses object detection and tracking algorithms to assess pedestrian safety. The primary objectives of the research were threefold: first, to assess pedestrian safety; second, to predict the severity of conflicts between pedestrians and vehicles; and third, to examine the effects of various factors pertaining to pedestrian, vehicle, and signal timing-related factors on the severity of pedestrian-vehicle conflicts. The fixed cycle lasts 60s and includes a 35-second green phase, a 15-second yellow phase, and a 20-second red phase for vehicles. The RRFB system at the second location is set to flash yellow during the next 15 seconds once a pedestrian has engaged it.

YOLOv4 was used due to its exceptional accuracy and efficiency in detecting and localizing objects, including pedestrians and vehicles, in video frames. In conjunction with YOLOv4, DeepSORT was used to ensure the continuity of pedestrians and tracking of pedestrians and vehicles across multiple frames. By associating detected pedestrians across frames, DeepSORT facilitated a seamless tracking process, enabling the analysis of pedestrian behavior and the identification of potential conflicts with vehicles. Only pedestrians and vehicles with consistent IDs were considered in this research.

Such detection and tracking algorithms can be integrated with the vehicle's communication systems. This integration allows for a real-time exchange of information between vehicles, infrastructure, and pedestrians, enabling a proactive and cooperative approach to safety. For instance, when a CAV detects a pedestrian in its vicinity, it can communicate this information to other vehicles, alerting them to the presence of the pedestrian and facilitating collaborative collision avoidance.

The research specifically targeted two intersections for analysis: a signalized intersection with a fixed cycle time and another intersection controlled by an RRFB. The objective was to examine pedestrian-vehicle conflicts within the crosswalk zones of these intersections. The fixed cycle time implies a predetermined duration for each traffic signal phase, including the time allocated for pedestrians to cross the intersection safely. RRFBs are a type of pedestrian-activated warning system with flashing lights installed near the crosswalk. Pedestrians can activate the flashing lights to alert drivers to their presence and indicate their intention to cross.

Macroscopic and microscopic validation was conducted using Kinovea software to ensure the validity of the generated trajectories, speeds, and PETs computed for the two intersections. Microscopic validation refers to comparing automatically and manually extracted trajectories, while macroscopic validation involves comparing pedestrian and vehicle speeds.

Three levels of severity of pedestrian-vehicle conflicts were defined based on the existing literature. The first level of severity, referred to as no conflict, for pedestrian-vehicle interactions where the PET exceeded 6s. In such cases, the duration of exposure between pedestrians and vehicles was considered sufficient for safe crossing, indicating a low risk of conflicts. The second level of severity, labeled as slight conflict, encompassed pedestrian-vehicle conflicts with a PET greater than 3s but not exceeding 6s. This range indicated a relatively shorter duration of exposure, indicating a potential crash risk. While conflicts may be less severe compared with the no conflict category, there is still a need to address safety concerns in these scenarios. The third and most severe level, severe conflict, involved pedestrian-vehicle interactions with a PET of 3s or less. In this category, the duration of exposure between pedestrians and vehicles was significantly limited, indicating a higher risk of a crash.

The following sections summarize the findings, provide recommendations for safety improvements, and propose a scope for future research.

8.1. Summary of Findings

8.1.1. Summary of Findings from the Pedestrian Safety Assessment

The findings reveal important insights into the severity of pedestrian-vehicle conflicts at the fixed-cycle intersection and the RRFB-controlled intersection. Here is a summary of the key findings.

- *Total conflicts at the fixed-cycle intersection*. Out of the observed 744 pedestrians, 238 pedestrians (about 32%) were involved in conflicts with vehicles while crossing the road, as indicated by PET values of less than 6 seconds.
- *Total conflicts at the RRFB-controlled intersection*. Out of the observed 1,083 pedestrians, 511 pedestrians (about 47% of all conflicts) were involved in conflicts with vehicles, as indicated by PET values of less than 6 seconds.
- *Jaywalking conflicts at the fixed-cycle intersection*. Among the observed conflicts, 55 instances (about 23% of conflicts) involved jaywalkers. This suggests that jaywalking pedestrians contribute substantially to conflicts at the intersection.
- *Jaywalking conflicts at the RRFB-controlled intersection*. Among the conflicts observed, 218 instances (about 43% of conflicts) involved jaywalkers. This indicates that conflicts with jaywalkers are an important contributor to conflicts at the RRFB-controlled intersection.

8.1.2. Summary of the Prediction of Pedestrian-Vehicle Conflict Severity

LSTM neural network models were developed for the two intersections to predict the severity of pedestrian-vehicle conflicts based on pedestrian, vehicle, and signal timing factors. LSTM neural networks were preferred as they effectively capture temporal dependencies and pedestrian and vehicle trajectories. The proposed LSTM neural network model architectures for both models comprise three stacked LSTM layers, one dense layer, and two dropout layers. The main differences between the two models lie in the signal timing-related factors used as variables and the selected values of parameters considered after model tuning.

- The LSTM neural network model developed for the fixed-cycle intersection exhibited good performance, as indicated by its AUC value of 81.7% on the training dataset, showcasing its discriminatory capabilities in predicting the three levels of conflict severity involving pedestrians and vehicles. Furthermore, the model achieved recall values of 74.7% and 68.9% on the test dataset for slight and severe conflicts, respectively, resulting in an overall recall rate of 76.7%, accounting for no conflicts as well.
- For the RRBF-controlled intersection, the AUC value reached 78.5% on the training dataset. The recall values on the test dataset for slight and severe conflicts were 74.8% and 66.5%, respectively. The overall recall value accounting for the three levels of pedestrian-vehicle conflict severity was 71.1%.

8.1.3. Summary of the Effects on Pedestrian-Vehicle Conflict Severity

An adjacent-category approach was used to model the effects of pedestrian, vehicle, and signal timing factors on the severity of pedestrian-vehicle conflicts at the fixed-cycle intersection and at the RRFB-controlled intersection. The following summarizes the findings.

- *Pedestrian-related factors at the fixed-cycle intersection*. Compared with a non-conflict situation, pedestrian red-light violations increase the likelihood of a slight conflict by 5.9%. Jaywalking is more likely to increase the severe conflict situation by 9.5% compared with a slight conflict situation.
- *Pedestrian-related factors at the RRFB-controlled intersection*. The likelihood of a slight conflict with a vehicle increases by 17.1% if a pedestrian decides to jaywalk. Moreover, the likelihood of a severe conflict with a vehicle increases by 17.8% when compared with a slight conflict situation
- *Vehicle-related factors at the fixed-cycle intersection*. Driving at a speed greater than 25 mph increases the likelihood of a slight conflict by about 24.7% compared with a non-conflict situation. Similarly, the likelihood of a severe conflict increases by 13.1% compared with the slight conflict situation.
- *Vehicle-related factors at the RRFB-controlled intersection*. A slight conflict is about 12.0% more likely to occur on the adjacent vehicle lanes compared with a non-conflict situation. Driving at a speed greater than the 20-mph speed limit affects the severity of pedestrian-vehicle conflicts the same way (same directions of the effect) as the fixed-cycle intersection.
- *Signal timing-related factors at the fixed-cycle intersection*. A one-second increase in yellow time can decrease the likelihood of a slight conflict situation by 17.2% when compared with a non-conflict situation. On the other hand, a one-second increase in yellow time can decrease the likelihood of a severe conflict situation by about 20.9% when compared with a slight conflict situation.

- *Signal timing-related factors at the RRBF-controlled intersection*. Compared with a non-conflict (slight conflict) situation, the likelihood of a slight (severe) pedestrian-vehicle conflict decreases by 21.3% (19.3%) if the RRFB flashing time increased by 1s.

8.2. Recommendations

This research highlights the potential of object detection and tracking algorithms, such as YOLOv4 and DeepSORT, in improving traffic safety. Further development and refinement of these algorithms can lead to more accurate and reliable detection and tracking of pedestrians and vehicles, thereby enhancing overall safety measures.

The developed LSTM neural network models for the fixed-cycle intersection and the RRBF-controlled intersection have the potential for real-time prediction of pedestrian-vehicle conflict severities. By leveraging the continuous monitoring and analysis of pedestrian and vehicle movements, the models can provide timely insights into potential conflicts, allowing for proactive safety measures and interventions. The models allow to predict pedestrian-vehicle conflict severities 2s before pedestrians enter the conflict zone.

The findings emphasize the importance of paying close attention to signal timing at both signalized intersections with fixed cycle lengths and at locations with RRFBs. This highlights the need for careful analysis and optimization of signal phasing and timings to ensure adequate pedestrian crossing time, minimize conflicts, and maximize overall safety for pedestrians and vehicles. Increasing the yellow time at fixed-cycle intersections and the duration of the flashing time at RRBF-controlled intersections can significantly enhance pedestrian safety and reduce the likelihood of conflicts and crashes.

8.3. Scope for Future Research

The challenges and safety implications of multimodal interactions and strategies to mitigate conflicts will enhance overall safety in shared spaces. Therefore, the research can be extended by investigating the complex interactions between pedestrians, vehicles, and other modes of transportation, such as bicycles and scooters.

Technology and analytical capabilities are growing at a rapid pace. Such big data analytics and predictive modeling techniques can be explored to integrate large-scale datasets from multiple sources, including traffic cameras, vehicle sensors, and pedestrian counting systems. It will help better allocate resources and enhance safety by identifying high-risk areas, predicting conflicts, and optimizing safety interventions.

Only fixed cycle signalized intersection and RRFB-controlled intersection are explored in this research. The pedestrian-vehicle interactions and safety at other intersection control types differ from these intersection controls. Understanding the dynamics and safety implications of different intersection types can help develop comprehensive guidelines and strategies for enhancing pedestrian-vehicle interactions in diverse urban environments. Such intersection control types include uncontrolled intersections, roundabouts, protected and unprotected left turn intersections, and unconventional intersection designs. There is a need to extend this research by analyzing the unique challenges and safety considerations associated with each type of intersection and proposing tailored solutions to mitigate conflicts and improving pedestrian safety.

REFERENCES

1. Afshari, A., Ayati, E., & Barakchi, M. (2021). Evaluating the effects of external factors on pedestrian violations at signalized intersections (a case study of Mashhad, Iran). *IATSS Research, 45*(2), 234-240.
2. Agbelie, B. R., & Roshandeh, A. M. (2015). Impacts of signal-related characteristics on crash frequency at urban signalized intersections. *Journal of Transportation Safety & Security, 7*(3), 199-207.
3. Ali, Y., Haque, M. M., & Mannering, F. (2023). A Bayesian generalised extreme value model to estimate real-time pedestrian crash risks at signalised intersections using artificial intelligence-based video analytics. *Analytic Methods in Accident Research, 38*, 100264.
4. Alhajyaseen, W. K., & Iryo-Asano, M. (2017). Studying critical pedestrian behavioral changes for the safety assessment at signalized crosswalks. *Safety Science*, *91*, 351-360.
5. Anderson, J. A. (1984). Regression and ordered categorical variables. *Journal of the Royal Statistical Society: Series B (Methodological), 46*(1), 1-22.
6. Arbel, N. (2018). How LSTM networks solve the problem of vanishing gradients. *Medium, December*.
7. Arvind, C. S., Jyothi, R., Mahalakshmi, K., Vaishnavi, C. K., & Apoorva, U. (2019). Vision based driver assistance for near range obstacle sensing under unstructured traffic environment. *IEEE Symposium Series on Computational Intelligence*,1163-1170.
8. Bewley, A., Ge, Z., Ott, L., Ramos, F., & Upcroft, B. (2016). Simple online and realtime tracking. *IEEE International Conference on Image Processing (ICIP)*, 3464-3468.
9. Bochkovskiy, A., Wang, C. Y., & Liao, H. Y. M. (2020). Yolov4: optimal speed and accuracy of object detection. *arXiv preprint arXiv:*2004.10934.

10. Bonneson, J. A., & Zimmerman, K. H. (2004). Effect of yellow-interval timing on the frequency of red-light violations at urban intersections. *Transportation Research Record*, *1865*(1), 20-27.
11. Bradbury, K., Stevens, J., Boyle, L. N., & Rutherford, S. (2012). To go or not to go: Pedestrian behavior at intersections with standard pedestrian call buttons. *Transportation Research Record*, *2299*(1), 174-179.
12. Chahal, K. S., & Dey, K. (2018). A survey of modern object detection literature using deep learning. *arXiv preprint arXiv:*1808.07256.
13. Charmant, J. et al., (2021). Kinovea 0.9.5. .
14. Chaudhari, A., Gore, N., Arkatkar, S., Joshi, G., & Pulugurtha, S. (2021). Exploring pedestrian surrogate safety measures by road geometry at midblock crosswalks: A perspective under mixed traffic conditions. *IATSS Research*, *45*(1), 87-101.
15. Chawla, N. V., Bowyer, K. W., Hall, L. O., & Kegelmeyer, W. P. (2002). SMOTE: synthetic minority over-sampling technique. *Journal of Artificial Intelligence Research*, *16*, 321-357.
16. Chen, L., Chen, C., & Ewing, R. (2014). The relative effectiveness of signal related pedestrian countermeasures at urban intersections—Lessons from a New York City case study. *Transport Policy*, *32*, 69-78.
17. Dangeti, M. R., Pulugurtha, S. S., Vasudevan, V., Nambisan, S. S., & White, O. C. (2010). Evaluating ITS-based countermeasures: How effective are they in enhancing pedestrian safety. *89th Annual Meeting of the Transportation Research Board*.
18. Diependaele, K. (2019). Non-compliance with pedestrian traffic lights in Belgian cities. *Transportation Research Part F: Traffic Psychology and Behaviour*, *67*, 230-241.

19. Duduta, N., Zhang, Q., & Kroneberger, M. (2014). Impact of intersection design on pedestrians' choice to cross on red. *Transportation Research Record*, *2464*(1), 93-99.
20. Ewing, R., & Dumbaugh, E. (2009). The built environment and traffic safety: a review of empirical evidence. *Journal of Planning Literature*, *23*(4), 347-367.
21. Färber, B. (2016). Communication and communication problems between autonomous vehicles and human drivers. *Autonomous Driving*, 125-144.
22. Formosa, N., Quddus, M., Ison, S., Abdel-Aty, M., & Yuan, J. (2020). Predicting real-time traffic conflicts using deep learning. *Accident Analysis & Prevention*, *136*, 105429.
23. Fu, T., Hu, W., Miranda-Moreno, L., & Saunier, N. (2019). Investigating secondary pedestrian-vehicle interactions at non-signalized intersections using vision-based trajectory data. *Transportation Research Part C: Emerging Technologies*, *105*, 222-240.
24. Fu, T., Miranda-Moreno, L., & Saunier, N. (2016). Pedestrian crosswalk safety at nonsignalized crossings during nighttime: Use of thermal video data and surrogate safety measures. *Transportation Research Record*, *2586*(1), 90-99.
25. Fuest, T., Sorokin, L., Bellem, H., & Bengler, K. (2017). Taxonomy of traffic situations for the interaction between automated vehicles and human road users. *In International Conference on Applied Human Factors & Ergonomics*, 708-719.
26. Fullerton, A. S., & Anderson, K. F. (2021). Ordered regression models: A tutorial. *Prevention Science*, 1-13.
27. Girshick, R., Donahue, J., Darrell, T., & Malik, J. (2014). Rich feature hierarchies for accurate object detection and semantic segmentation. *Proceedings of the IEEE Conference on Computer Vision and Pattern Recognition*, 580-587.

28. Goodman, L. A. (1983). The analysis of dependence in cross-classifications having ordered categories, using log-linear models for frequencies and log-linear models for odds. *Biometrics,* 149-160.
29. Gough, M. (2016). Machine smarts: How will pedestrians negotiate with driverless cars? *The Guardian*. Accessed on December 10, 2021.
30. Granié, M. A. (2007). Gender differences in preschool children's declared and behavioral compliance with pedestrian rules. *Transportation Research Part F: Traffic Psychology and Behaviour*, *10*(5), 371-382.
31. Green, O., Ivan, J. N., Filipovska, M., Auguste, M. E., & Wang, K. (2023). Using Logistic Regression to Evaluate Pedestrian–Vehicle Interaction Severity at Side Street Green and Exclusive Phase Signals. *Transportation Research Record*, 03611981231159120.
32. Haddington, P., & Rauniomaa, M. (2014). Interaction between road users: Offering space in traffic. *Space & Culture*, *17*(2), 176-190.
33. Hashemi, H., Bargegol, I., & Hamedi, G. H. (2022). Using logistic regression and point-biserial correlation, an investigation of pedestrian violations and their opportunities to cross at signalized intersections. *IATSS Research*, *46*(3), 388-397.
34. Hochreiter, S., & Schmidhuber, J. (1997). Long short-term memory. *Neural Computation*, *9*(8), 1735-1780.
35. Holland, C., & Hill, R. (2007). The effect of age, gender and driver status on pedestrians' intentions to cross the road in risky situations. *Accident Analysis & Prevention*, *39*(2), 224-237.

36. Hubbard, S. M., Bullock, D. M., & Mannering, F. L. (2009). Right turns on green and pedestrian level of service: Statistical assessment. *Journal of Transportation Engineering*, *135*(4), 153-159.

37. Hu, L., Hu, X., Che, Y., Feng, F., Lin, X., & Zhang, Z. (2020a). Reliable state of charge estimation of battery packs using fuzzy adaptive federated filtering. *Applied Energy*, *262*, 114569.

38. Hu, L., Hu, X., Wan, J., Lin, M., & Huang, J. (2020b). The injury epidemiology of adult riders in vehicle-two-wheeler crashes in China, Ningbo, 2011–2015. *Journal of Safety Research*, *72*, 21-28.

39. Hu, L., Ou, J., Huang, J., Wang, F., Wang, Y., Ren, B., ... & Zhou, L. (2022). Safety evaluation of pedestrian-vehicle interaction at signalized intersections in Changsha, China. *Journal of Transportation Safety & Security*, *14*(10), 1750-1775.

40. Hussein, M., Sayed, T., Reyad, P., & Kim, L. (2015). Automated pedestrian safety analysis at a signalized intersection in New York City: Automated data extraction for safety diagnosis and behavioral study. *Transportation Research Record*, *2519*(1), 17-27.

41. Iryo-Asano, M., Alhajyaseen, W. K., & Nakamura, H. (2014). Analysis and modeling of pedestrian crossing behavior during the pedestrian flashing green interval. *IEEE Transactions on Intelligent Transportation Systems*, *16*(2), 958-969.

42. Islam, M. S., Serhiyenko, V., Ivan, J. N., Ravishanker, N., & Garder, P. E. (2014). Explaining pedestrian safety experience at urban and suburban street crossings considering observed conflicts and pedestrian counts. *Journal of Transportation Safety & Security*, *6*(4), 335-355.

43. Jana, A. P., & Biswas, A. (2018). YOLO based detection and classification of objects in video records. *IEEE International Conference on Recent Trends in Electronics, Information & Communication Technology*, 2448-2452.

44. Jensen, O. B. (2010). Negotiation in motion: Unpacking a geography of mobility. *Space & Culture*, *13*(4), 389-402.

45. Jiang, X., Wang, W., Mao, Y., Bengler, K., & Bubb, H. (2011). Situational factors of influencing drivers to give precedence to jaywalking pedestrians at signalized crosswalk. *International Journal of Computational Intelligence Systems*, *4*(6), 1407-1414.

46. Ka, D., Lee, D., Kim, S., & Yeo, H. (2019). Study on the framework of intersection pedestrian collision warning system considering pedestrian characteristics. *Transportation Research Record*, *2673*(5), 747-758.

47. Karimpour, A., Jalali Khalilabadi, P., Homan, B., Wu, Y. J., & Swartz, D. L. (2023). Modeling red-light running behavior using high-resolution event-based data: a finite mixture modeling approach. *Journal of Intelligent Transportation Systems*, 1-16.

48. Karkee, G., Pulugurtha, S. S., & Nambisan, S. S. (2006). Evaluating the effectiveness of turning traffic must yield to pedestrians (R 10-15) sign. *Applications of Advanced Technology in Transportation*, 400-405.

49. Kathuria, A., & Vedagiri, P. (2020). Evaluating pedestrian vehicle interaction dynamics at un-signalized intersections: a proactive approach for safety analysis. *Accident Analysis & Prevention*, *134*, 105316.

50. Koller-Meier, E.B., & Ade, F. (2001). Tracking multiple objects using the Condensation algorithm. *Robotics and Autonomous Systems*, 34, 93–105.

51. Krishna, N. M., Reddy, R. Y., Reddy, M. S. C., Madhav, K. P., & Sudham, G. (2021). Object detection and tracking using Yolo. *IEEE Third International Conference on Inventive Research in Computing Applications (ICIRCA)*, 1-7.
52. Lehsing, C., Fleischer, M., & Bengler, K. (2016). On the track of social interaction: A non-linear quantification approach in traffic conflict research. In *2016 IEEE 19th International Conference on Intelligent Transportation Systems (ITSC)*, 2046-2051.
53. Li, P., Abdel-Aty, M., Cai, Q., & Islam, Z. (2020). A deep learning approach to detect real-time vehicle maneuvers based on smartphone sensors. *IEEE Transactions on Intelligent Transportation Systems*, *23*(4), 3148-3157.
54. Lin, J. P., & Sun, M. T. (2018). A YOLO-based traffic counting system. *Conference on Technologies and Applications of Artificial Intelligence*, 82-85.
55. Lin, T. Y., Maire, M., Belongie, S., Hays, J., Perona, P., Ramanan, D., Dollar, P., & Zitnick, C. L. (2014). Microsoft COCO: Common objects in context. *European Conference on Computer Vision*, 740-755.
56. Long, J. S., & Cheng, S. (2004). Regression models for categorical outcomes. *Handbook of Data Analysis*, 259-284.
57. Manual on uniform traffic control devices (MUTCD). (2009). *United States Department of Transportation, Federal Highway Administration*.
58. Milan, A., Leal-Taixé, L., Reid, I., Roth, S., & Schindler, K. (2016). MOT16: A benchmark for multi-object tracking. *arXiv preprint arXiv:1603.00831*.
59. Nambisan, S. S., Pulugurtha, S. S., Vasudevan, V., Dangeti, M. R., & Virupaksha, V. (2009). Effectiveness of automatic pedestrian detection device and smart lighting for pedestrian safety. *Transportation Research Record*, *2140*(1), 27-34.

60. National Center for Statistics and Analysis (NCSA). (2020). Preview of motor vehicle traffic fatalities in 2019. *National Highway Traffic Safety Administration*. Report No. DOT HS 813 021, United States Department of Transportation.
61. Obeid, H., Abkarian, H., Abou-Zeid, M., & Kaysi, I. (2017). Analyzing driver-pedestrian interaction in a mixed-street environment using a driving simulator. *Accident Analysis & Prevention*, *108*, 56-65.
62. Porter, B. E., & England, K. J. (2000). Predicting red-light running behavior: a traffic safety study in three urban settings. *Journal of Safety Research*, *31*(1), 1-8.
63. Pulugurtha, S. S., Agurla, M., & Khader, K. S. C. (2011). How effective are flashing yellow arrow signals in enhancing safety?. *Transportation and Development Institute Congress, Integrated Transportation and Development for a Better Tomorrow*, 1096-1104.
64. Pulugurtha, S. S., Desai, A., & Pulugurtha, N. M. (2010a). Are pedestrian countdown signals effective in reducing crashes?. *Traffic Injury Prevention*, *11*(6), 632-641.
65. Pulugurtha, S. S., Nambisan, S. S., Dangeti, M. R., & Vasudevan, V. (2010b). Evaluation of effectiveness of traffic signs to enhance pedestrian safety. *89th Transportation Research Board Annual Meeting*, 10-1016.
66. Pulugurtha, S. S., Nambisan, S. S., & Maheshwari, P. (2006). Estimating pedestrian counts in urban areas for transportation planning and safety analyses. *Applications of Advanced Technology in Transportation*, 257-262.
67. Pulugurtha, S. S., & Otturu, R. (2014). Effectiveness of red light running camera enforcement program in reducing crashes: Evaluation using before the installation, after the installation, and after the termination data. *Accident Analysis & Prevention*, *64*, 9-17.

68. Pulugurtha, S. S., & Repaka, S. R. (2008). Assessment of models to measure pedestrian activity at signalized intersections. *Transportation Research Record, 2073*(1), 39-48.

69. Pulugurtha, S. S., & Self, D. R. (2015). Pedestrian and motorists' actions at pedestrian hybrid beacon sites: findings from a pilot study. *International Journal of Injury Control & Safety Promotion*, *22*(2), 143-152.

70. R Core Team (2021). R: A language and environment for statistical computing. R Foundation for Statistical Computing, Vienna, Austria. https://www.R-project.org/.

71. Radwan, E., Darius, B., Wu, J., & Abou-Senna, H. (2016). Simulation of pedestrian safety surrogate measures. In *ARRB Conference, 27th, Melbourne, Victoria, Australia*.

72. Rasouli, A., & Tsotsos, J. K. (2018). Joint attention in driver-pedestrian interaction: from theory to practice. *arXiv preprint arXiv:*1802.02522.

73. Rasouli, A., Yau, T., Rohani, M., & Luo, J. (2020b). Multi-modal hybrid architecture for pedestrian action prediction. *arXiv preprint arXiv:*2012.00514.

74. Redmon, J., Divvala, S., Girshick, R., & Farhadi, A. (2016). You only look once: Unified, real-time object detection. *Proceedings of The IEEE Conference on Computer Vision & Pattern Recognition*, 779-788.

75. Ren, S., He, K., Girshick, R., & Sun, J. (2015). Faster R-CNN: Towards real-time object detection with region proposal networks. *Advances In Neural Information Processing Systems*, *28*.

76. Retting, R. A., Ferguson, S. A., & Farmer, C. M. (2008). Reducing red light running through longer yellow signal timing and red-light camera enforcement: results of a field investigation. *Accident Analysis & Prevention*, *40*(1), 327-333.

77. Rosén, E., & Sander, U. (2009). Pedestrian fatality risk as a function of car impact speed. *Accident Analysis & Prevention*, *41*(3), 536-542.

78. Rosenbloom, T., Nemrodov, D., & Barkan, H. (2004). For heaven's sake follow the rules: pedestrians' behavior in an ultra-orthodox and a non-orthodox city. *Transportation Research Part F: Traffic Psychology and Behaviour*, *7*(6), 395-404.

79. Schmidt, S., & Faerber, B. (2009). Pedestrians at the kerb: Recognising the action intentions of humans. *Transportation Research Part F: Traffic Psychology & Behaviour*, *12*(4), 300-310.

80. Sedgwick, P. (2014). One way analysis of variance: post hoc testing. *BMJ Publishing Group*, *349*, g7067.

81. Singh, S. (2015). Critical reasons for crashes investigated in the national motor vehicle crash causation survey. Report No. DOT HS 812 115, United States Department of Transportation.

82. Singh, M. K., Pathivada, B. K., Rao, K. R., & Perumal, V. (2022). Driver behaviour modelling of vehicles at signalized intersection with heterogeneous traffic. *IATSS Research*, *46*(2), 236-246.

83. Song, Y. E., Lehsing, C., Fuest, T., & Bengler, K. (2018). External HMIs and their effect on the interaction between pedestrians and automated vehicles. *International Conference on Intelligent Human Systems Integration*,13-18.

84. Sucha, M., Dostal, D., & Risser, R. (2017). Pedestrian-driver communication and decision strategies at marked crossings. *Accident Analysis & Prevention*, *102*, 41-50.

85. Tarko, A. P. (2018). Surrogate measures of safety. In Safe mobility: challenges, methodology and solutions *Emerald Publishing Limited*, 11, 383-405.

86. Varhelyi, A. (1998). Drivers' speed behaviour at a zebra crossing: a case study. *Accident Analysis & Prevention*, *30*(6), 731-743.

87. Vasudevan, V., Pulugurtha, S. S., Nambisan, S. S., & Dangeti, M. R. (2011). Effectiveness of signal-based countermeasures for pedestrian safety: Findings from pilot study. *Transportation Research Record*, *2264*(1), 44-53.

88. Wang, T., Cardone, G., Corradi, A., Torresani, L., & Campbell, A. T. (2012). Walksafe: A pedestrian safety app for mobile phone users who walk and talk while crossing roads. *Proceedings of The Twelfth Workshop on Mobile Computing Systems & Applications*, 1-6.

89. Wilson, T. B., Butler, W., McGehee, D. V., & Dingus, T. A. (1997). Forward-looking collision warning system performance guidelines. *SAE Transactions*, 701-725.

90. Wojke, N., Bewley, A., & Paulus, D. (2017). Simple online and realtime tracking with a deep association metric. *IEEE International Conference on Image Processing (ICIP)*, 3645-3649.

91. Wu, Y., Abdel-Aty, M., Zheng, O., Cai, Q., & Yue, L. (2019). Developing a crash warning system for the bike lane area at intersections with connected vehicle technology. *Transportation Research Record*, *2673*(4), 47-58.

92. Yang, Y., & Sun, J. (2013). Study on pedestrian red-time crossing behavior: integrated field observation and questionnaire data. *Transportation Research Record*, *2393*(1), 117-124.

93. Zaki, M. H., & Sayed, T. (2014). Automated analysis of pedestrians' nonconforming behavior and data collection at an urban crossing. *Transportation Research Record*, *2443*(1), 123-133.

94. Zangenehpour, S., Miranda-Moreno, L. F., & Saunier, N. (2015). Automated classification based on video data at intersections with heavy pedestrian and bicycle traffic: Methodology and application. *Transportation Research Part C: Emerging Technologies*, *56*, 161-176.

95. Zhang, J., Vinkhuyzen, E., Cefkin, M. (2017). Evaluation of an autonomous vehicle external communication system concept: a survey study. *In International Conference on Applied Human Factors & Ergonomics*, 650-661.

96. Zhang, S., & Abdel-Aty, M. (2022). Real-time pedestrian conflict prediction model at the signal cycle level using machine learning models. *IEEE Open Journal of Intelligent Transportation Systems*, *3*, 176-186.

97. Zhang, S., Abdel-Aty, M., Cai, Q., Li, P., & Ugan, J. (2020a). Prediction of pedestrian-vehicle conflicts at signalized intersections based on long short-term memory neural network. *Accident Analysis & Prevention*, *148*, 105799.

98. Zhang, S., Abdel-Aty, M., Wu, Y., & Zheng, O. (2021). Pedestrian crossing intention prediction at red-light using pose estimation. *IEEE Transactions on Intelligent Transportation Systems*, *23*(3), 2331-2339.

99. Zhang, S., Abdel-Aty, M., Wu, Y., & Zheng, O. (2020b). Modeling pedestrians' near-accident events at signalized intersections using gated recurrent unit (GRU). *Accident Analysis & Prevention*, *148*, 105844.

100. Zhang, Y., Mamun, S. A., Ivan, J. N., Ravishanker, N., & Haque, K. (2015). Safety effects of exclusive and concurrent signal phasing for pedestrian crossing. *Accident Analysis & Prevention*, *83*, 26-36.

101. Zhou, Z. P., Liu, Y. S., Wang, W., & Zhang, Y. (2013). Multinomial logit model of pedestrian crossing behaviors at signalized intersections. *Discrete Dynamics in Nature and Society*, *2013*.

102. Zhuang, X., & Wu, C. (2014). Pedestrian gestures increase driver yielding at uncontrolled mid-block road crossings. *Accident Analysis & Prevention*, *70*, 235-244.